

國立臺灣大學醫學院分子醫學研究所

碩士論文

Institute of Molecular Medicine

College of Medicine

National Taiwan University

Master Thesis



線蟲神經系統調控粒線體壓力反應的分子機制

Neural Regulation of Mitochondrial Stress Response in
Caenorhabditis elegans

林志達

Chih-Ta Lin

指導教授：潘俊良 博士

Advisor: Chun-Liang Pan, M.D., Ph.D.

中華民國 105 年 7 月

July, 2016





國立臺灣大學碩士學位論文

口試委員會審定書

線蟲神經系統調控粒線體壓力反應的分子機制

Neural Regulation of Mitochondrial Stress Response in

Caenorhabditis elegans

本論文係 林志達君 (R03448012) 在國立臺灣大學分子醫學研究所完成之碩士學位論文，於民國 105 年 6 月 29 日承下列考試委員審查通過及口試及格，特此證明

口試委員：

李俊良

(簽名)

(指導教授)

許財樹

吳益群

系主任、所長

李俊良

(簽名)




ACKNOWLEDGEMENT



研究所的生涯終於快到了尾聲，在分醫所的七百多個日子是如此的充實與深刻，絲毫不敢怠慢。感謝實驗室的學長姊：姜浩菁、徐均旻以及潘俊良老師(Peter)一同幫助我完成本篇的著作研究。並且要感謝台大生科院的吳益群老師和陽明生科院生化所的許翹麟老師以及我的指導教授潘俊良老師(Peter)擔任我的口試委員，在每次的報告中，提供論文的研究方向與建議，使這篇研究能朝向好的方向。

特別要感謝 Peter 的用心栽培與指導，從 Peter 身上看見了一個優秀科學家對於科學研究的熱忱與執著，同時也是對於學生無比付出與關懷的老師。仍然記得第一次聽 Peter 介紹 Lab 的研究和生活，可以感受到實驗室就是個大家庭，各自有各自的研究，卻在 Peter 用心的領導下緊密的相連，對於彼此的研究都有相當程度的瞭解；剛進到線蟲世界的懵懂無知，透過 Peter 有耐心的從線蟲最基本的知識與實驗技術的介紹，使線蟲成為我生活中的一份子。Peter 總是不厭其煩在每一次進度報告前一頁頁的替我修改簡報，改錯、補充、修飾，深化我的背景知識與英文表達能力，引領我進入科學的世界，也不吝嗇給予我們生活和想法上的幫助和建議。同時，感謝 Peter 給我機會前往日本參加線蟲神經會議，和世界頂尖的科學家交流，聽取他們的研究成果，並且指導我貼海報展現我的研究成果，對於我的碩士班生涯留下深刻和美好的回憶。若沒有 Peter 的鼓勵和幫助，我從未想過能夠有今天的成果，Pan Lab 讓這一切成真，而這一切都要歸功於 Peter 的指導。

謝謝浩菁學姊和均旻學長兼同梯教導我線蟲相關的基本實驗、概念和知識，同時也提供了整個 FZO-1 研究的方向，有了你們奠定的基礎與努力，才有我今天的研究成果。再來，謝謝小黑學長、彥志學長，身為 Pan Lab 的三本柱，不時給予我實驗或是未來規劃上的協助，在對於科學的態度和對於未來的準備，也是我



們的好榜樣；還有健博學長、虹蓁學姊、奎延學長，很喜歡和你們討論課業上的疑問或是實驗上的困難，亦或是日常生活上的閒聊，豐富了實驗室的生活；還有我的好同學俊緯、子庭和半個成員梅均，同樣身為 Pan Lab 的成員，互相討論和扶持，一起努力在科學的世界中學習，透過閒聊和一起出遊更增進大家的感情；以及學妹良憶和欣穎，實驗室有你們的加入也變得更多元又熱鬧，也補足實驗室少數的女生。

最後，我要感謝我的家人，給予我極大的鼓勵和支持，讓我無後顧之憂地徜徉在科學的大海中，沒有你們，就沒有現在的我。還有很多一路上幫助我的人，我真心感謝與珍惜這得來不易的機會，以及能讓我好好學習的環境。感謝 Peter 和 Pan Lab 的各位，這裡所學一生受用。

志達

2016.7

中文摘要



逆境或外在壓力導致生物體內蛋白構型異常時，細胞會透過專一性的訊號傳遞機制，進行各不同胞器獨特的生理反應，藉以去除構型異常的失能蛋白或將蛋白的構型恢復正常，這些統稱為胞器內未摺疊蛋白反應 (UPR)，其中包含了細胞質的熱休克反應(HSR)和內質網(UPR^{ER})和粒線體的未摺疊蛋白反應(UPR^{mt})。生物體的老化會造成蛋白恆定態的失衡或粒線體功能異常，除伴隨著細胞生理功能的下降，也可能引起異常的未摺疊蛋白反應。前人在秀麗桿狀線蟲 *Caenorhabditis elegans* 當中發現，神經細胞內粒線體的呼吸狀態會影響線蟲全身性的粒線體蛋白平衡，但是神經細胞內與不同細胞間訊息傳遞的分子機制尚不清楚。本篇研究發現線蟲中調控粒線體融合的蛋白 FZO-1/Mitofusin 可以影響粒線體未折疊蛋白反應。*fzo-1* 基因的突變引發多形性的性狀，包含生長遲緩、生殖能力下降、神經老化加速和粒線體未摺疊蛋白反應的異常上升。我們發現在神經細胞內專一表現 FZO-1，除可以改善神經內粒線體型態的缺失和神經元細胞的過度老化外，亦可以有效改善 *fzo-1* 突變所引發的全身性粒線體未摺疊蛋白反應的異常上升，及減緩 *fzo-1* 突變所引發的生長遲緩。在腸道內專一表現 FZO-1 則可改善粒線體未摺疊蛋白反應在腸細胞內的異常上升。本篇研究發現神經細胞內粒線體型態的調控可以影響全身粒線體蛋白的平衡，有助於了解神經細胞內粒線體如何透過訊號傳遞來調控全身粒線體蛋白的平衡和生物體老化過程中蛋白質的恆定性。

關鍵字：線蟲；粒線體；粒線體融合蛋白 FZO-1/Mitofusin；未摺疊蛋白反應；神經訊號

ABSTRACT



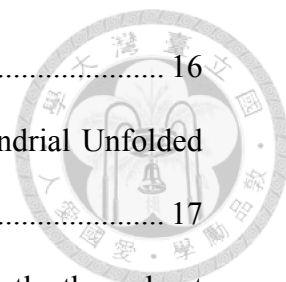
Compartment-specific stress responses, including cytosolic heat shock response (HSR), the endoplasmic reticulum unfolded protein response (UPR^{ER}), and the mitochondrial unfolded protein response (UPR^{mt}), protect animals against proteotoxic stress. Age-dependent decline in cellular functions and organismal physiology is associated with dysregulated protein homeostasis and mitochondrial function. Systemic proteostasis in the nematode *Caenorhabditis elegans* could be regulated by mitochondrial respiration in the neurons, but the molecular mechanisms of such intercellular control of protein homeostasis remains unclear. Here we report that the *C. elegans* mitochondrial fusion protein FZO-1/Mitofusin controlled UPR^{mt} in a cell non-autonomous manner. Mutations of *fzo-1* caused pleiotropic phenotypes, including slow development, reduced fecundity, accelerated neuronal aging, and maladapted UPR^{mt}. Neuronal mitochondrial defects and aging signs of the neurites were rescued by neuron-autonomous FZO-1 functions. The maladapted UPR^{mt} in the intestine was moderately rescued by intestinal FZO-1 expression. Unexpectedly, aberrant intestinal UPR^{mt} of the *fzo-1* mutants was significantly ameliorated by neuronal FZO-1. Neuronal FZO-1 also partially rescued the slow development of the *fzo-1* mutant. We are now exploring neuron-derived signals that potentially mediate such non-autonomous effects on systemic mitochondrial proteostasis. Progress in this proposal could further our understanding of how mitochondria-mediated, neuron-derived signals control systemic protein homeostasis and cellular aging at the organismal level.

Key words: *C. elegans*, Mitochondria, FZO-1/Mitofusin, Unfolded protein response, Neuronal signal

CONTENTS



口試委員會審定書.....	#
ACKNOWLEDGEMENT	i
中文摘要.....	iii
ABSTRACT.....	iv
CONTENTS.....	v
Chapter 1 INTRODUCTION.....	1
1.1 FZO-1/Mitofusins and Mitochondrial Dynamics	2
1.2 Regulation of Mitochondrial Proteome Homeostasis: the UPR ^{mt}	3
1.3 Cell Non-Autonomous UPR ^{mt} Regulation.....	5
1.4 Current Study: Neuronal Mitochondrial Dynamics and Systemic UPR ^{mt} Regulation.....	6
Chapter 2 MATERIALS and METHODS.....	9
2.1 <i>C. elegans</i> Strains and Genetics.....	9
2.2 Brood Size and Development Test.....	10
2.3 Feeding RNA Interference	10
2.4 Single Molecule RNA Fluorescence in situ Hybridization (smFISH).....	11
2.5 Quantification of Heat Shock Responses of GFP-Based Stress Reporters..	11
2.6 Fluorescence Microscopy and Quantification of Fluorescence Signal.....	12
2.7 Oxygen Consumption Assay.....	12
2.8 Mitochondrial Morphology.....	12
Chapter 3 RESULTS.....	15
3.1 Mutations of <i>fzo-1</i> /Mitofusin Caused Pleiotropic Defects in <i>C. elegans</i>	15



3.2	Mitochondrial and Neuronal Defects in the <i>fzo-1</i> Mutant	16
3.3	The <i>fzo-1</i> Mutation Specifically Induced Aberrant Mitochondrial Unfolded Protein Response.....	17
3.4	Mutations of <i>fzo-1</i> Triggered Maladapted UPR ^{mt} Consistently throughout Development.....	19
3.5	Mitochondrial Fragmentation Triggered Systemic UPR ^{mt}	20
3.6	<i>fzo-1</i> Functions Autonomously and Non-autonomously to Regulate Systemic UPR ^{mt}	21
3.7	Loss of Neuronal <i>fzo-1</i> Triggers Systemic UPR ^{mt} Via Neurotransmitters and Neuropeptides	23
Chapter 4	DISCUSSION	25
4.1	Communication of Neurons with Distal Tissues in the Regulation of Stress Responses.....	26
4.2	The Physiological Significance of UPR ^{mt}	27
Chapter 5	FIGURES	29
	Figure 1. Characterization of the <i>fzo-1</i> mutant.....	30
	Figure 2. Pleiotropic defects in the <i>fzo-1</i> mutant.	32
	Figure 3. Mitochondria in the touch neurons were fragmented in the <i>fzo-1</i> mutant.....	34
	Figure 4. Mitochondrial morphology is regulated by FZO-1.	36
	Figure 5. Mitochondria in the intestine were fragmented in the <i>fzo-1</i> mutant.....	38
	Figure 6. The <i>fzo-1</i> mutant showed robust UPR^{mt} induction in early adulthood.....	40

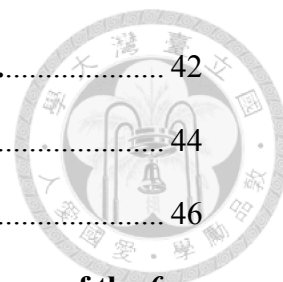


Figure 7. The <i>fzo-1</i> mutant showed intact UPR ^{ER} activation.....	42
Figure 8. The <i>fzo-1</i> mutant showed intact HSR activation.....	44
Figure 9. <i>fzo-1</i> knockdown induced maladapted UPR ^{mt}	46
Figure 10. <i>hsp-6</i> transcripts were increased in somatic tissues of the <i>fzo-1</i> mutant.....	48
Figure 11. The <i>fzo-1</i> mutant showed increased <i>hsp-60</i> expression.....	50
Figure 12. Maladapted UPR ^{mt} in the <i>fzo-1</i> mutant requires canonical UPR ^{mt} genes.	52
Figure 13. UPR ^{mt} is constitutively activated throughout embryogenesis and larval development in the <i>fzo-1</i> mutant.....	54
Figure 14. UPR ^{mt} activation persisted during aging in the <i>fzo-1</i> mutant.	56
Figure 15. <i>fzo-1</i> mutation may induce maladapted UPR ^{mt} in part through respiratory inhibition.....	58
Figure 16. Mitochondrial dynamics influenced respiration.....	60
Figure 17. Mitochondrial dynamics controlled UPR ^{mt} activation.....	62
Figure 18. Intestine-specific <i>fzo-1</i> knockdown triggered UPR ^{mt}	64
Figure 19. Muscle-specific <i>fzo-1</i> knockdown did not induce UPR ^{mt}	66
Figure 20. Intestine-specific <i>cco-1</i> knockdown triggered UPR ^{mt} induction.....	68
Figure 21. Muscle-specific <i>cco-1</i> knockdown failed to induce UPR ^{mt}	70
Figure 22. Neuron-specific <i>fzo-1</i> knockdown triggered UPR ^{mt}	72
Figure 23. Tissue-specific <i>fzo-1</i> expression and the rescue of UPR ^{mt}	74
Figure 24. Intestinal mitochondrial fragmentation were partially rescued by tissue-specific FZO-1 expression.....	76

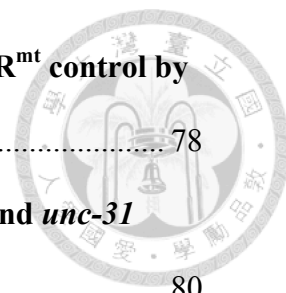


Figure 25. Models of autonomous and non-autonomous UPR^{mt} control by FZO-1.	78
Figure 26. <i>cco-1</i> knockdown induced UPR^{mt} in the <i>unc-13</i> and <i>unc-31</i> mutants.	80
Figure 27. Cell non-autonomous induction of UPR^{mt} requires both neurotransmitters and neuropeptides.	82
Figure 28. Model of systemic UPR^{mt} regulation by <i>fzo-1</i> in the neurons. ..	84
Chapter 6 REFERENCE	87

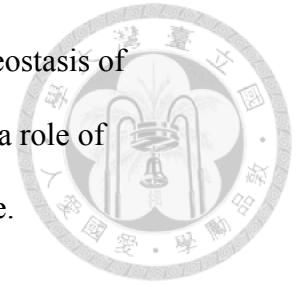
Chapter 1 INTRODUCTION



Aging involves widespread decline in systemic homeostasis of physiology and metabolism across diverse tissues. Mitochondria, the crucial cellular power plant for ATP synthesis, are implicated broadly in aging in addition to their many cellular functions, such as the regulation of apoptosis, and Ca^{2+} signaling (Dillin et al., 2002; Ferri and Kroemer, 2001; Jiang et al., 2015; Rizzuto and Pozzan, 2006). Functions of the mitochondria are intimately associated with their dynamics in morphology, which transits between tubular, interconnected network and isolated, fragmented profiles (Chan, 2012). Progressive fragmentation of mitochondria is found during aging of diverse organisms (Hughes and Gottschling, 2012; Jiang et al., 2015; Roux et al., 2016; Scheckhuber et al., 2007; Yasuda et al., 2006), confirming that mitochondrial deterioration is a universal hallmark for cellular aging.

Given these lines of well-documented evidence suggesting mitochondria deterioration as a consequence of aging, it thus appears counterintuitive that inhibition of mitochondrial respiration extends *Caenorhabditis. elegans* life span (Dillin et al., 2002), an observation that implicates mitochondria as a contributor and regulator of aging in addition to being substrates for aging. A provocative but rarely attended question is how regulation of mitochondrial morphology is coupled with aging, and whether mitochondrial dynamics in any particular tissue coordinates systemic homeostasis of organismal physiology or metabolism. Here I will briefly review mechanisms that regulate mitochondrial dynamics. I then move the focus to *fzo-1*, the *C. elegans* homolog of mammalian Mitofusins, critical regulators of mitochondrial fusion and contacts between mitochondria and the endoplasmic reticulum (ER). I

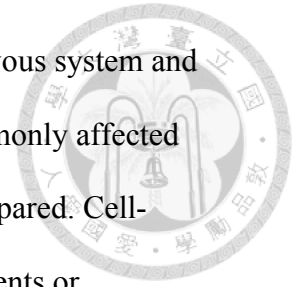
discuss recent advances in the regulatory mechanisms for systemic homeostasis of mitochondrial proteome, and elaborate our preliminary data implicating a role of neuronal *fzo-1* in cell-nonautonomous control of mitochondrial proteome.



1.1 FZO-1/Mitofusins and Mitochondrial Dynamics

Mitochondrial dynamics are primarily controlled by large GTPases that bear structural and sequence similarities to dynamins, a class of GTPases that cleave membrane during endocytosis. Dynamin-related protein 1 (Drp1/DRP-1) promotes mitochondrial fission, whereas Mitofusins/FZO-1 and Optic atrophy 1 (OPA1/EAT-3) regulate fusion of the outer and inner mitochondrial membrane, respectively. The mammalian Mitofusin 2 (MFN2) additionally regulates contact between mitochondria and ER, although the exact role that MFN2 plays here remains debated (de Brito and Scorrano, 2008; Filadi et al., 2015). Unlike the two Mitofusins in mammals subserving distinct functions, FZO-1 is the sole *C. elegans* Mitofusin that is equally similar to MFN2 and MFN1 in peptide sequence. *fzo-1* mutants show mitochondrial fragmentation in *C. elegans* embryonic cells, body wall muscles, intestine and neurons (Breckenridge et al., 2008; Jiang et al., 2015; Johnson and Nehrke, 2010), confirming its role in promoting mitochondrial fusion in *C. elegans*. Mutations in *Mfn2* are the most common cause for Charcot-Marie-Tooth disease type 2A, a form of severe hereditary motor and sensory axonal neuropathy characterized by severe muscle atrophy, axon degeneration and sensory loss (Rossor et al., 2013; Zuchner et al., 2004). Although mitochondrial fragmentation could be found in sural nerves from symptomatic patients and transgenic mice bearing MFN2(R94Q), a frequent *Mfn2* mutation in severe CMT2A (Cartoni et al., 2010; Verhoeven et al., 2006), mechanistic links between *Mfn2* mutations and axon

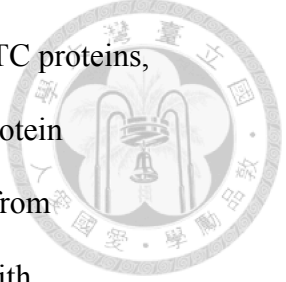
degeneration have been elusive. In particular, neurons in the central nervous system and myocardium, two tissues that consume oxygen at high rate and are commonly affected in diseases bearing mutations in the mitochondrial genome, are largely spared. Cell-nonautonomous effects of *Mfn2* mutations had not been explored in patients or experimental models.



1.2 Regulation of Mitochondrial Proteome Homeostasis: the UPR^{mt}

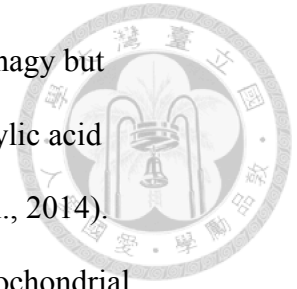
Compartment-specific stress responses are protective mechanisms that maintain homeostasis of proteome under intrinsic or environmental stress by reducing and eliminating misfolded proteins and fine-tuning protein synthesis (Walter and Ron, 2011). Prominent examples include cytosolic heat shock response and unfolded protein response of the ER (UPR^{ER}), which achieve homeostasis of the cellular proteome via induction of molecular chaperones, activation of protein degradation machineries and inhibition of translation (Balch et al., 2008). The mitochondrial unfolded protein response (UPR^{mt}) is unique in that it represents a signaling cascade that communicates the mitochondrial genome with the nuclear genome, aiming to restore homeostasis of the mitochondrial proteome under mitochondrial stress (Haynes and Ron, 2010). Here I will focus on UPR^{mt} for the rest of this thesis.

Components of the electron transport chain (ETC) complexes at the mitochondrial inner membrane are encoded by both the nuclear and mitochondrial genomes. Since surplus ETC subunits that fail to be assembled into functional ETC complexes are potential sources of misfolded proteins, it is critical to coordinate the activity of the nuclear and mitochondrial genomes to achieve optimal stoichiometry of ETC components with minimal uncomplexed ETC proteins. Conditions that



compromise ETC functions result in the accumulation of unassembled ETC proteins, which triggers UPR^{mt} to reduce mitochondrial protein import, increase protein turnover in the mitochondrial matrix, and reprogram cellular respiration from oxidative phosphorylation to glycolysis. This enables the stressed cells with compromised mitochondria to keep producing ATP, albeit at lower level with suboptimal efficiency. In the meanwhile UPR^{mt} initiates cascades of molecular and signaling events that clear the mitochondrial matrices of unfolded proteins and stimulate mitochondrial biogenesis, aiming to compensate for compromised respiration of pre-existing mitochondria.

Regulation of UPR^{mt} is best understood in *C. elegans*, where this signaling cascade was first described (Yoneda et al., 2004). At the mechanistic level, induction of the UPR^{mt} converges on the master transcription factor, activating transcription factor associated with stress-1 (ATFS-1), that shuttles between the mitochondria and nucleus (Nargund et al., 2012). ATFS-1 has N-terminal sequence that targets the mitochondrial matrix, and C-terminal sequence that directs the protein to the nucleus. Under nonstressful conditions, ATFS-1 is constantly imported into the mitochondrial matrix through transporters on the inner and outer mitochondrial membranes (the TIM/TOM protein complexes), where it is degraded by the Lon protease (Chacinska et al., 2009; Hill et al., 1998; Nargund et al., 2012). In the presence of stressors that compromise ETC functions and reduce respiration, degradation of ATFS-1 is downregulated, coupled with a blockade of ATFS import mediated in part by the mitochondrial ABC peptide transporter HAF-1 (Haynes et al., 2010; Young et al., 2001). The impact of alteration in ATFS-1 levels and distribution is two-fold. First, ATFS-1 is redirected to the nucleus via the C-terminus nuclear localizing signal,

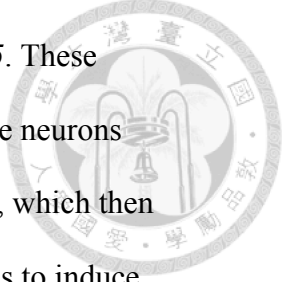


where it activates genes for glycolysis, antimicrobial peptides and autophagy but represses genes for oxidative phosphorylation (OXPHOS) and tricarboxylic acid (TCA) cycle (Nargund et al., 2015; Nargund et al., 2012; Pellegrino et al., 2014). Second, undegraded ATFS-1 in the mitochondrial matrix targets the mitochondrial genome and represses OXPHOS genes, similar to what it does to the nuclear genome (Nargund et al., 2015). In the nucleus, the ubiquitin-like protein UBL-5 and transcriptional co-activator DVE-1 act with ATFS-1 to reprogram nuclear genome transcription (Benedetti et al., 2006; Haynes et al., 2007). Recently, ATFS-1 had been shown to directly stimulate mitochondrial biogenesis under stress (Lin et al., 2016), a possible compensatory reaction to circumvent dysfunctional mitochondria by generating freshly new mitochondria with proper ETC stoichiometry.

1.3 Cell Non-Autonomous UPR^{mt} Regulation

Perturbation of mitochondrial respiration, if occurs early in life, extends the adult life span of *C. elegans* (Dillin et al., 2002). While the temporal requirement of this ETC-related longevity remains largely mysterious, recent studies pinpoint UPR^{mt} as a mediator of ETC-based longevity (Durieux et al., 2011). ETC inhibition by knocking down cytochrome c oxidase/*cco-1*/COX4 extends life span and triggers robust UPR^{mt} (Durieux et al., 2011). Importantly, elimination of *ubl-5* largely suppressed the longevity conferred by mitochondrial inhibition, suggesting that mediates ETC-based longevity (Durieux et al., 2011).

Interestingly, Durieux et al., observed that ETC inhibition specifically in the neuron also prolongs *C.elegans* lifespan and triggers systemic UPR^{mt} induction in the intestine (Durieux et al., 2011), and unlike ETC inhibition in non-neural tissues,

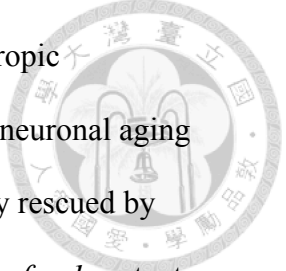


longevity conferred by neuronal ETC inhibition does not depend on *ubl-5*. These observations indicate the existence of unknown diffusible signals from the neurons that are produced and secreted as a reaction to neuronal respiratory stress, which then target distal tissues directly or indirectly via intervening neurons or tissues to induce UPR^{mt}.

In fact, it had been shown that heat shock responses (HSR) in *C. elegans* require the thermosensory circuit (Prahlad et al., 2008; Tatum et al., 2015). Animals whose AFD thermosensory neurons are genetically ablated or inactivated show compromised HSR (Prahlad et al., 2008). A follow-up study reveals that the AFD acts through serotonergic ADF neurons secretion to regulate systemic HSR (Tatum et al., 2015), strengthening the idea that neurons modulate systemic HSR via secreted signals. Similarly, in *C. elegans*, systemic UPR^{ER} could be induced by overexpression of XBP-1, a key transcriptional regulator of UPR^{ER}, in the neurons (Taylor and Dillin, 2013), and this non-autonomous UPR^{ER} induction extends life span. A recent study links neuronal AMPK signaling to longevity via catecholamine (octopamine and tyramine in *C. elegans*) (Burkewitz et al., 2015). These studies support the model that in *C. elegans*, the nervous system secretes neurotransmitters or neuropeptides to regulate systemic homeostasis of proteome integrity cell non-autonomously, and this neurohormonal control of proteome homeostasis impacts aging and life span. However, neuromodulators that regulate systemic UPR^{mt} and UPR^{ER} remain unknown.

1.4 Current Study: Neuronal Mitochondrial Dynamics and Systemic UPR^{mt} Regulation

Here I report that the *C. elegans* mitochondrial fusion protein FZO-1/Mitofusin controls



UPR^{mt} in a cell non-autonomous manner. Mutations of *fzo-1* cause pleiotropic phenotypes, including slow development, reduced fecundity, accelerated neuronal aging and maladapted UPR^{mt}. The maladapted UPR^{mt} in the intestine is partially rescued by intestinal FZO-1 expression. Surprisingly, aberrant intestinal UPR^{mt} of the *fzo-1* mutants is significantly ameliorated by neuronal FZO-1. Neuronal FZO-1 also partially rescued the slow development of the *fzo-1* mutant. I further confirm tissues of action of UPR^{mt} induction by cell-specific *fzo-1* RNAi. Mutations that block neurotransmitter or neuropeptide secretion partially suppress maladapted UPR^{mt} in the *fzo-1* mutant, implicating secreted neuronal signals in the regulation of UPR^{mt} in distal tissues. I discuss possible mechanisms that link FZO-1-dependent regulation of mitochondrial dynamics to ETC function and systemic UPR^{mt} induction.



Chapter 2 MATERIALS and METHODS



2.1 *C. elegans* Strains and Genetics

Strains were cultured at 20°C as described (Brenner, 1974), and the following *C.*

elegans alleles and transgenes were used in the current study:

LG I: unc-13(e1091)

LG II: fzo-1(tm1133), eat-3(ad426)

LG IV: drp-1(tm1108), unc-31(e928)

fzo-1(tm1133) was outcrossed at least three times before use. The following transgenes or strains were used:

zcIs4(Phsp-4::GFP)/V,

zcIs13(Phsp-6::GFP)/V,

zcIs9(Phsp-60::GFP, lin-15(+))/V,

dvIs70[Phsp-16.2::GFP, rol-6(su1006)],

VP303[rde-1(ne219)/V; kbIs7(Pnhx-2::RDE-1), rol-6(su1006)],

WM118[rde-1(ne300)/V; neIs9(Pmyo-3::HA::RDE-1), rol-6(su1006)],

twnEx220(Pmec-7::GFP::Mfn2, Pmec-7::mito::mCherry),

twnEx229(Pmec-7::GFP::fzo-1, Pmec-7::mito::mCherry),

twnEx320(Punc-119::dsfzo-1(RNAi), Punc-119::mCherry),

twnEx321(Punc-119::fzo-1(50ng), Punc-119::mCherry),

twnEx322(Phsp-6::GFP, Pgcy-8::mCherry),

twnEx323(Pelt-2::fzo-1(30ng), Pelt-2::NLS::tagBFP),

twnEx324(Pfzo-1::fzo-1(20ng), Pgcy-8::mCherry, Pelt-2::NLS::tagBFP),

twnEx325(Phsp-6::GFP, Pgcy-8::mCherry),

twnEx326(Phsp-6::GFP, Pgcy-8::mCherry). Germline transformation by microinjection was carried out as described (Mello et al., 1991).

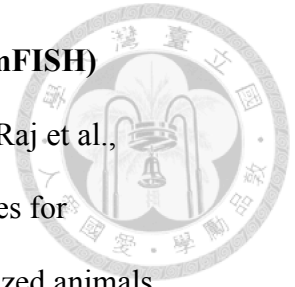


2.2 Brood Size and Development Test

For assaying brood size, animals were incubated at 20°C and a single gravid hermaphrodite was allowed to lay embryos for 24 hours before transferred to a new plate. The egg plate was scored 24 hours later for larvae that successfully hatched. Analysis was carried out for the first four days of adulthood. For assaying development, synchronized early L1 animals were fed with OP50 or HT115 *E. coli* strains and allowed to develop for 48 or 54 hours, and were quantified for the percentage of animals successfully reaching L4 or young adult, respectively.

2.3 Feeding RNA Interference

Feeding RNAi was performed as described (Kamath et al., 2001). We used HT115 *E. coli* strains containing dsRNA-expressing plasmids, ampicillin-selected and grew them overnight in 2X YT liquid culture (1% yeast extract, 1.6% tryptone, 0.5% NaCl) with 75 µg/ml ampicillin at 37°C. Next, bacteria were diluted 100 folds and incubated at 37°C for 3 hours. Isopropyl-thiogalactopyranoside (IPTG) was added to a final concentration of 1 mM, and the culture was incubated at 37°C with shaking for 1 hours before 100 µl of such liquid culture was seeded on IPTG/ampicillin-containing NGM plates. These RNAi plates were then dried at room temperature overnight before use. Each RNAi experiment was repeated at least three times.

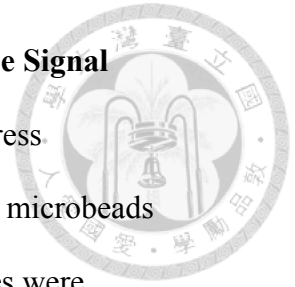


2.4 Single Molecule RNA Fluorescence in situ Hybridization (smFISH)

Probe design and hybridization was performed as previously described (Raj et al., 2008) (see also Wormbook and www.singlemoleculefish.com). All probes for hybridization were coupled to Quasar 670 (Cy5 replacement). Synchronized animals were grown on NGM plates with OP50 at 20°C until L3 stage. Animals were collected, washed by M9 and fixed with 4% paraformaldehyde in 1X PBS for 45 minutes. After washed twice with 1X PBS, fixed worms were processed in 70% ethanol overnight at 4°C. Hybridization was performed with 20% formamide overnight at 30°C in dark. Animals were then mounted with 2XSSC and ProLong Gold Antifade Reagent (Invitrogen) and counter-stained with DAPI for image analysis. Confocal were taken for single plane images, with DAPI identified as intestinal nucleus localization. Only the mRNA spots that were visible in neighboring sections were counted to exclude false positive signals.

2.5 Quantification of Heat Shock Responses of GFP-Based Stress Reporters

For assaying compartment-specific stress responses, *Phsp-16.2::GFP* (for HSR), *Phsp-4::GFP* (for UPR^{ER}) or *Phsp-6::GFP* (for UPR^{mt}) were used. D1 animals with *Phsp-16.2::GFP* or *Phsp-6::GFP* were heat-shocked at 34°C for 6 hours without food, respectively. The *Phsp-16.2::GFP* animals were cultured on FUdR plate, and mock treatment at 20°C was performed as a control. For *Phsp-4::GFP* (UPR^{ER}) induction, D1 animals were treated with 25ng/μl tunicamycin (Sigma) or 6.25μM dithiothreitol (DTT) (Sigma) in M9 buffer for 4 hours, respectively.



2.6 Fluorescence Microscopy and Quantification of Fluorescence Signal

For epifluorescence or fluorescent confocal microscopy, animals with stress reporters were anesthetized with 1% sodium azide. 1mM levamisole and microbeads were used to immobilize animals with *GFP::*Mfn2** or *GFP::*fzo-1**. Images were acquired using the Zeiss AxioImager2 or Zeiss LSM700 confocal imaging system. Animals were manually aligned for imaging. Pixel intensities of the regions of interest were quantified using ImageJ with subtraction of background signals.

2.7 Oxygen Consumption Assay

For measuring oxygen consumption rate (OCR) in living *C. elegans* we used the Seahorse apparatus with 24-well plates (with kind assistance from Dr. Szecheng Lo of Chang Gung University, Taiwan). The Seahorse Bioscience XF24 Extracellular Flux Analyzer program measured the OCR with the following protocol: 1-calibrate probes; 2-loop 10 times; 3-mix 2 min; 4-time delay 2 min; 5-measure 2 min; 6-loop end. Synchronized animals were grown on NGM plates with OP50 at 20°C until D1 stage. One hundred adult animals were collected and washed twice with M9. Animals were then transferred to the Seahorse assay plate with 500 µl M9 buffer.

2.8 Mitochondrial Morphology

Animals were cultured on NGM plates seeded with OP50 containing 100nM fluorescent dye tetramethylrhodamine ethyl ester (TMRE) (Invitrogen) for overnight at 20°C. Worms were then transferred to fresh OP50 plates without TMRE for 1 hour to clean their intestinal tract of residual dye, and animals were anesthetized

with 1mM levamisole and microbeads. Mitochondria were visualized by the Zeiss LSM700 confocal imaging system.





Chapter 3 RESULTS



3.1 Mutations of *fzo-1*/Mitofusin Caused Pleiotropic Defects in *C. elegans*

To examine the roles of Mitofusins in *C. elegans* development and physiology, we focused on *fzo-1*, which encodes the sole *C. elegans* Mitofusin. Nucleotide sequence analysis suggested that *fzo-1* showed comparable similarity to either human *Mfn1* or *Mfn2* genes. The only available *fzo-1* mutant allele, *tm1133*, was an insertion-deletion (Indel) that had 419 base pair (bp) of *fzo-1* sequence missing and 14 bp insertion of uncertain origin (Figure 1A). Previous studies confirmed that mitochondria in *C. elegans* embryonic cells, body wall muscles and neurons were severely fragmented in the *fzo-1* mutant, consistent with it being a regulator for mitochondrial fusion (Breckenridge et al., 2008; Ichishita et al., 2008; Jiang et al., 2015; Rolland et al., 2009). To examine its significance in *C. elegans* development or physiology, we further characterized progression through larval stages as well as fecundity in the *fzo-1* mutant. Most wild-type newly-hatched larvae (early L1) reached the last larval stage (L4) after growing for 48 hours at 20°C, whereas only about 30% of the *fzo-1* animals reached L4 48 hours after hatching (Figure 2A). Even at 72 hours post-hatching, when all wild-type animals became fertile adults, 80% of the *fzo-1* animals remained in the larval stage (data not shown). These data suggested a severe delay of larval development in the *fzo-1* mutant. To assess fecundity, we quantified the number of viable embryos laid in the first four days of adulthood, a period when adult worms lay most of their embryos. This analysis showed that, the *fzo-1* mutant produced much fewer viable embryos compared to the wild type, likely due to sterility or early

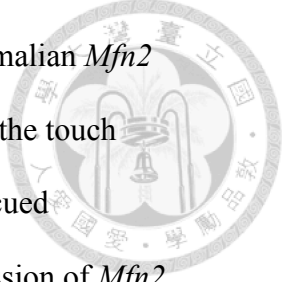
embryonic lethality (Figure 2B). Together these observations confirm that mutations in *fzo-1* significantly compromised development and fecundity of *C. elegans*.



3.2 Mitochondrial and Neuronal Defects in the *fzo-1* Mutant

The six touch mechanosensory neurons that sense light touch in *C. elegans* include the bilaterally symmetric ALM and PLM in the anterior and posterior, respectively, and the PVM on the left and the AVM on the right. We and others previously reported that *C. elegans* showed age-dependent defects in these touch receptor neurons, including abnormal neuronal morphology and progressive mitochondrial fragmentation (Jiang et al., 2015; Pan et al., 2011; Tank et al., 2011; Toth et al., 2012). Here we further investigated whether neuronal and mitochondrial morphology was affected by *fzo-1* mutations. To visualize mitochondria in live animals, we fused mCherry with TOMM-20, a mitochondrial outer membrane protein, and expressed the TOMM-20::mCherry (referred to as “mito::mCherry” hereafter) transgene in the touch neurons from the *mec-7* promoter (Figure 3). We classified mitochondrial morphology into four categories: Grade 0, all mitochondria showed networked morphology; Grade 1, most mitochondria being in networked morphology with < 50% (in terms of the cytosolic area of the neuron observed) mitochondria fragmented; Grade 2, > 50% mitochondria showing fragmentation; Grade 3, completely fragmented mitochondria (Figure 3). According to these semi-quantitative criteria, we found that mitochondria in the touch neurons were mostly fused in young adult, and were progressively fragmented during aging (Figure 3). By contrast, in the *fzo-1* mutant, neuronal mitochondria were mostly fragmented since early adulthood (Figure 3).

Nucleotide sequence analysis (Figure 1B) suggested that *fzo-1* was equally similar

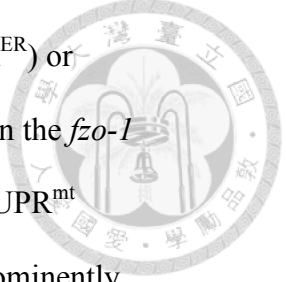


to mammalian *Mfn1* and *Mfn2* genes. Here we determined whether mammalian *Mfn2* and *C. elegans fzo-1* were functionally conserved. Expression of *fzo-1* in the touch neurons, from the touch neuron-specific *mec-7* promoter, completely rescued mitochondrial fragmentation of the *fzo-1* mutant (Figure 4A). Overexpression of *Mfn2* in the touch neurons also rescued mitochondrial fragmentation in the *fzo-1* mutant with comparable efficiency (Figure 4A). Moreover, overexpression of either *fzo-1* or *Mfn2* significantly reduced mitochondrial fragmentation in the touch neurons of old wild-type animals (Figure 4A). GFP-tagged FZO-1 or MFN2 localized to the mitochondria when expression in the neurons (Figure 4B). These observations indicate that *C. elegans fzo-1* and mammalian *Mfn2* are functionally conserved.

In addition to neuronal mitochondria, we visualized mitochondria in the body wall muscles and the intestine, by the fluorescent dye tetramethylrhodamine ethyl ester (TMRE) (Ehrenberg et al., 1988). In the wild type, the intestinal mitochondria showed tubular, interconnected morphology (Figure 5). Similar to mitochondria in the touch neurons, intestinal and muscle mitochondria in the *fzo-1* mutant were completely fragmented and appeared swollen (Figure 5).

3.3 The *fzo-1* Mutation Specifically Induced Aberrant Mitochondrial Unfolded Protein Response

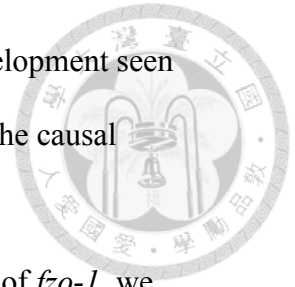
Previous studies indicated that mammalian MFN2, a key protein for maintaining appropriate contact between the mitochondria and the endoplasmic reticulum (ER), modulated ER stress response (Filadi et al., 2015; Munoz et al., 2013). As the pleiotropic defects in growth and fecundity of the *fzo-1* mutant could be a consequence of maladapted stress responses, we next determined whether compartment-specific



stress responses, including the unfolded protein response of the ER (UPR^{ER}) or mitochondria (UPR^{mt}), or the heat shock response (HSR), were aberrant in the *fzo-1* mutant. We used an *hsp-6p::GFP* transgene to monitor the activation of UPR^{mt} reporter as previously reported (Yoneda et al., 2004), which was most prominently expressed in the intestine upon UPR^{mt} induction (Figure 6). Transcription of *hsp-6* requires ATFS-1, the master transcription factor for UPR^{mt} induction that shuttles between the mitochondria and nucleus by specific targeting sequences, and also transcriptional co-regulators UBL-5 and DVE-1 (Benedetti et al., 2006; Haynes et al., 2007; Nargund et al., 2012). We found that *hsp-6p::GFP* was robustly induced in the *fzo-1* mutant without external stressors, in stark contrast to the barely detectable signals in the unstressed wild-type animals (Figure 6). By contrast, UPR^{ER} or HSR was not induced in the *fzo-1* mutant, judged by the *hsp-4p::GFP* and *hsp-16.2p::GFP* transgenes that monitor the induction of UPR^{ER} and HSR, respectively (Haynes et al., 2007; Prahlad et al., 2008) (Figure 7, 8). When worms were stimulated with specific stressors, such as 30C heat shock, dithiothreitol (DTT) (ER stressors) or 34C heat shock (heat stress), obvious *hsp-4p::GFP* and *hsp-16.2p::GFP* induction was seen both in the wild type and in the *fzo-1* mutant (Figure 7, 8). Taken together, these results suggest that the *fzo-1* mutation triggered maladapted UPR^{mt} but did not affect the capacity to respond to ER or heat stress.

fzo-1(tm1133) was an indel allele obtained by chemical mutagenesis. Although we outcrossed the strain several times to clean up the background, there is possibility that maladapted UPR^{mt} observed in *fzo-1(tm1133)* was caused by unknown mutations associated with *tm1133*. Therefore, we silenced *fzo-1* by feeding RNAi in the wild type. We found that UPR^{mt} was robustly induced by *fzo-1* RNAi (Figure 9A).

Moreover, *fzo-1* knockdown resulted in reduced fecundity and slow development seen in the *fzo-1(tm1133)* mutant (Figure 9B). These experiments confirmed the causal relationship between *fzo-1* loss and the induction of maladapted UPR^{mt}.

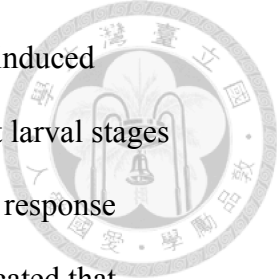


To obtain further proof that UPR^{mt} was indeed induced by the loss of *fzo-1*, we utilized single molecule mRNA in situ hybridization (smFISH) to detect *hsp-6* transcripts. In the wild-type L3 animals, *hsp-6* transcripts were barely detectable without stressors. By contrast, in the *fzo-1* mutant, we found that *hsp-6* transcripts were dramatically increased in somatic tissues (Figure 10). We further assayed for UPR^{mt} by observing *hsp-60p::GFP*, another established reporter for UPR^{mt} (Yoneda et al., 2004). The *hsp-60::GFP* was also robustly induced in the *fzo-1* mutant (Figure 11). Taken together, these results suggest that loss of *fzo-1* triggered maladapted UPR^{mt} in somatic tissues in *C. elegans*.

We next determined whether high *hsp-6p::GFP* expression in the *fzo-1* mutant required canonical UPR^{mt} genes. To test this, we knocked down classical UPR^{mt} genes, the transcriptional co-regulators *ubl-5* and *dve-1*, and the key transcription factor *atfs-1*, by feeding RNAi. The maladapted UPR^{mt} in the *fzo-1* mutant was significantly suppressed by knocking down *ubl-5*, *dve-1* and *atfs-1* (Figure 12). These results indicated that maladapted UPR^{mt} in the *fzo-1* mutant was triggered through a canonical UPR^{mt} pathway that required *ubl-5*, *dve-1* and *atfs-1*.

3.4 Mutations of *fzo-1* Triggered Maladapted UPR^{mt} Consistently throughout Development

We examined *hsp-6::GFP* activity from embryogenesis to late adulthood to determine whether maladapted UPR^{mt} was maintained throughout different stages in the life

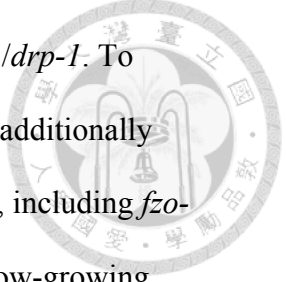


history of the *fzo-1* mutant. We found that *hsp-6p::GFP* was abnormally induced during embryogenesis (Figure 13A) and became progressively elevated at larval stages of the *fzo-1* mutant (Figure 13B). Furthermore, the aberrant *hsp-6p::GFP* response persisted during aging in the *fzo-1* mutant (Figure 14). These results indicated that loss of *fzo-1* triggered sustained maladapted UPR^{mt} in all life stages of the animal.

UPR^{mt} could be efficiently triggered by inhibiting mitochondrial electron transport chain (ETC) or perturbing turnover of the mitochondrial proteome (Dillin et al., 2002; Durieux et al., 2011; Haynes et al., 2007; Nolden et al., 2005; Yoneda et al., 2004). RNAi of the ETC complex IV component *cco-1* triggered robust UPR^{mt} (Figure 15). We found that oxygen consumption rate was reduced in the *fzo-1* mutant (Figure 16), suggesting that ETC function was compromised in the absence of *fzo-1*. In agreement of this, *fzo-1* animals showed slow development and reduced fecundity, two features that were shared by mutants with compromised ETC functions. This observation raised the possibility that maladapted UPR^{mt} arose in the *fzo-1* mutant as a consequence of mitochondrial respiratory failure. To test whether *fzo-1* acts genetically in the mitochondrial respiration to control UPR^{mt}, we silenced *cco-1* by feeding RNAi in the wild-type as well as in the *fzo-1* mutant. *cco-1* knockdown triggered robust UPR^{mt} induction in the wild type, which was not further enhanced in the *fzo-1* mutant (Figure 15). These results implied that *fzo-1* acted genetically in mitochondrial respiratory pathway to modulate systemic homeostasis of the mitochondrial proteome.

3.5 Mitochondrial Fragmentation Triggered Systemic UPR^{mt}

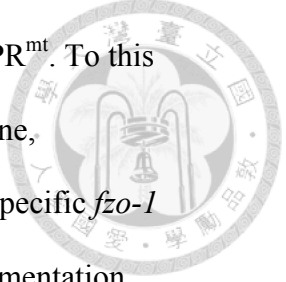
fzo-1 and *eat-3/Opa1*, another dynamin-related GTPases of the mitochondrial inner membrane, promote mitochondrial fusion. By contrast, fission of mitochondria is



mainly regulated by dynamin-related protein 1 of the large GTPase, Drp1/*drp-1*. To investigate whether mitochondrial dynamics broadly controls UPR^{mt}, we additionally assayed *Phsp-6::GFP* in the *eat-3* and *drp-1* mutants. Like other mutants, including *fzo-1*, with defective mitochondrial respiration, *eat-3* mutant animals were slow-growing and had reduced brood size (data not shown). Consistent with *eat-3* being required for mitochondrial ETC function, we found that oxygen consumption rate was reduced in the *eat-3* mutant (Figure 16). Surprisingly, the *eat-3* mutants also displayed robust *Phsp-6::GFP* induction, indicative of maladapted UPR^{mt} (Figure 17). By contrast, UPR^{mt} was only mildly activated by the *drp-1* mutation (Figure 17). Consistent with mitochondrial fusion, but not fission, being essential for ETC function, oxygen consumption rate was not affected in the *drp-1* mutant (Figure 16). These results indicate that proper activity of mitochondrial fusion ensures ETC-based mitochondrial respiration, and loss of mitochondrial fusion perturbs homeostasis of the mitochondrial proteome, resulting in sustained UPR^{mt} induction.

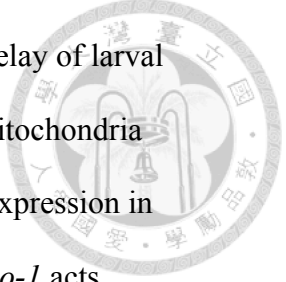
3.6 *fzo-1* Functions Autonomously and Non-autonomously to Regulate Systemic UPR^{mt}

Previous studies suggest that inhibition of mitochondrial respiration by *cco-1* knockdown extends life span likely by upregulating UPR^{mt} (Dillin et al., 2002; Durieux et al., 2011; Lee et al., 2003). Interestingly, tissue-specific *cco-1* knockdown in the intestine or the neurons triggers UPR^{mt} induction in the intestine and also extends life span (Durieux et al., 2011), suggesting that mitochondrial respiration modulates UPR^{mt} both autonomously and non-autonomously. Our results indicate that *fzo-1* modulates systemic UPR^{mt} through ETC-related mechanism. Therefore, we next



test whether tissue-specific *fzo-1* knockdown also modulates systemic UPR^{mt}. To this end, we used strains that are feeding RNAi-sensitive in muscles or intestine, respectively, and are otherwise RNAi-resistant in other tissues. Intestine-specific *fzo-1* knockdown triggered UPR^{mt} induction in the intestine, together with fragmentation and swelling of intestinal mitochondria, suggesting that *fzo-1* functions autonomously (Figure 18). By contrast, muscle-specific *fzo-1* knockdown failed to induce UPR^{mt} in the intestine, suggesting that *fzo-1* does not act non-autonomously in the muscles (Figure 19A). We ruled out the possibility that low RNAi efficiency in the muscles by showing that mitochondria became fragmented after *fzo-1* RNAi (Figure 19B). To confirm the tissue specificity of our RNAi strains, we knocked down *cco-1* as a control, and found that *cco-1* RNAi triggered UPR^{mt} in intestine-RNAi strain (Figure 20). By contrast, muscle-specific *cco-1* RNAi did not upregulate UPR^{mt} non-autonomously in the intestine (Figure 21). To test neurons are an important tissue from which *fzo-1* regulates intestinal UPR^{mt} non-autonomously, we drove double-strand *fzo-1* RNA from the pan-neuronal promoter *unc-119*. Neuronal *fzo-1* dsRNA expression also induced UPR^{mt} in the intestine, suggesting that *fzo-1* function in the neurons can non-autonomously modulate systemic UPR^{mt} (Figure 22).

To further substantiate these conclusions regarding tissue specificity of *fzo-1* functions in UPR^{mt} regulation, we further determine whether maladapted UPR^{mt} in the intestine could be rescued by tissues-specific *fzo-1* expression in the intestine or neurons. *fzo-1* expression from its own promoter or from the *elt-2* intestinal promoter partially rescued the maladapted UPR^{mt} (Figure 23). Overexpression of *fzo-1* in the neurons, using the *unc-119* promoter, also partially reduced the maladapted UPR^{mt}, consistent with *fzo-1* functioning non-autonomously from the neurons (Figure 23).



Importantly, neuronal *fzo-1* overexpression partially rescued the severe delay of larval development in the *fzo-1* mutant (Figure 23). Morphology of intestinal mitochondria was partially restored to become interconnected or tubular by *fzo-1* overexpression in the intestine or neurons (Figure 24). Together these results suggest that *fzo-1* acts autonomously in the intestine and non-autonomously in the neurons to modulate systemic UPR^{mt} and homeostasis of mitochondrial proteome.

3.7 Loss of Neuronal *fzo-1* Triggers Systemic UPR^{mt} Via Neurotransmitters and Neuropeptides

Our tissue-specific rescue and RNAi experiments with *fzo-1* pinpoint the nervous system as a critical site in modulating UPR^{mt} of the intestine in a cell non-autonomous manner. We hypothesize that loss of neuronal *fzo-1* induces systemic UPR^{mt} in distal tissues via secreted neurotransmitters or neuropeptides (Figure 25). To test this, we utilize the *unc-13* and *unc-31* mutations to block neurotransmitter or neuropeptide release, respectively. UNC-13 is required for synaptic vesicle (SV) fusion and release, which contains neurotransmitters. By contrast, UNC-31 is the *C. elegans* homolog for mammalian Ca²⁺-dependent activator protein for secretion (CAPS) and mediates the release of dense core vesicles (DCVs), which contain neuropeptides (Madison et al., 2005; Speese et al., 2007). The *unc-13* and *unc-31* animals responded normally to *cco-1* RNAi by inducing robust UPR^{mt} in the intestine (Figure 26), suggesting that they are not required for cell-autonomous UPR^{mt} induction. Strikingly, the maladapted UPR^{mt} of the *fzo-1* mutant was effectively reduced by both *unc-13* and *unc-31* mutations (Figure 27). These results suggest that upon *fzo-1* loss, the neurons secrete both neurotransmitters and neuropeptides to trigger systemic UPR^{mt} in distal tissues.



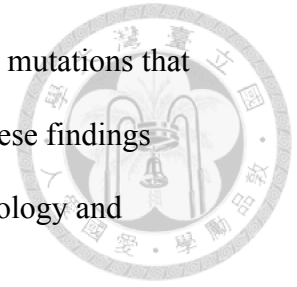
Chapter 4 DISCUSSION



Mitofusins are well known as a critical regulator of mitochondrial fusion and ER-mitochondrial contact (Mitofusin 2) (de Brito and Scorrano, 2008; Filadi et al., 2015).

In addition to these cell-autonomous functions, in mouse model of obesity, loss of Mitofusin in anorexigenic pro-opiomelanocortin (POMC) neurons in the hypothalamus triggers systemic leptin resistance and obesity through induction of neuronal ER stress responses, presumably due to loss of ER-mitochondrial contact (Schneeberger et al., 2013). Though not directly implicating Mitofusins, respiratory inhibition in the neurons extend life span in *C. elegans* through induction of systemic UPR^{mt} (Durieux et al., 2011; Merkwirth et al., 2016), further supporting the idea of non-autonomous regulation of organism-wide physiology by mitochondrial functions in the neurons. How neuronal mitochondria regulate systemic stress response in distal tissues remains unknown. Specifically, it remains completely elusive the identity of neuronally derived signals or modulators that serve this non-autonomous function. In our current study, we provide experimental evidence that neuronal FZO-1/Mitofusin controls UPR^{mt} in a cell non-autonomous manner in *C. elegans*. Loss of FZO-1 induces systemic, maladapted UPR^{mt} in the absence of stressors. Induction of UPR^{mt} in the intestine of the *fzo-1* mutant was partially ameliorated by intestinal FZO-1 expression, implicating cell-autonomous function of *fzo-1*. Strikingly, neuronal FZO-1 expression also reduced intestinal UPR^{mt} and raised the possibility of non-autonomous FZO-1 functions. This finding was confirmed by neuron-specific *fzo-1* knockdown. We also determine that genetically, loss of *fzo-1* triggers UPR^{mt} through a pathway shared by inhibition of mitochondrial respiration. Most important of all, we demonstrate that induction of maladapted UPR^{mt}

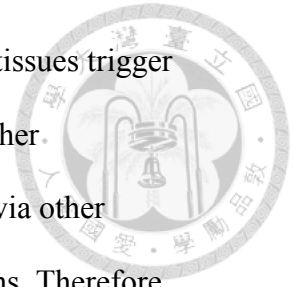
in the intestine requires secreted neurotransmitters and neuropeptides, as mutations that block the release of these neuronal signals significantly blunt UPR^{mt}. These findings open a new avenue in the research of neuronal control of systemic physiology and proteostasis through mitochondrial dynamics and respiration.



4.1 Communication of Neurons with Distal Tissues in the Regulation of Stress Responses

In *C. elegans*, the nervous system regulates systemic stress responses in distal tissues through secreted signals (Durieux et al., 2011; Tatum et al., 2015; Taylor and Dillin, 2013). An earlier study suggests that the AFD thermosensory neurons are essential for induction of systemic heat shock response (HSR) (Prahlad et al., 2008), and subsequent reports show that the AFD acts through two serotonergic neurons, ADF and NSM, to regulate systemic HSR (Tatum et al., 2015). In this recent study, HSR is monitored in the germline, which is not innervated. Therefore, these data are most consistent with that serotonergic neurons secrete serotonin to target germline tissues directly or indirectly via other neurons. Taylor and Dillin find that expression of XBP-1, a key transcription factor in the induction of UPR^{ER}, in the neurons triggers systemic UPR^{ER} and life span extension (Taylor and Dillin, 2013), which could be blocked by the *unc-13* mutation that disrupts synaptic vesicle fusion. This result implicates small molecule neurotransmitters as critical neuronal signals that trigger UPR^{ER} in distal tissues.

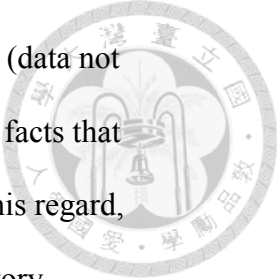
Burkewitz et al. suggest that tyramine and octopamine mediate the effects of perturbation of neuronal AMP kinase (AMPK) signaling on systemic mitochondrial homeostasis (Burkewitz et al., 2015). Consistent with these studies, we find that *C. elegans* neurons regulate systemic UPR^{mt} through released neurotransmitters and



neuropeptides. Intriguing questions include how distal, signal-receiving tissues trigger appropriate stress responses upon targeted by neuronal signals, and whether neurotransmitters reach distal target tissues via synapse-like contacts or via other intervening neurons. The *C. elegans* intestine is not innervated by neurons. Therefore, we favor the model that either neurotransmitters from nearby axonal terminals can diffuse over short distance to reach the intestinal cells, or neurotransmitters act on other, peptidergic neurons, which then release neuropeptides to target the intestine. Our data that blocking neuropeptide secretion partially ameliorates systemic UPR^{mt} indicate the importance of neuropeptides in non-autonomous control of mitochondrial stress response. A future challenge is the identification of such neurotransmitters and neuropeptides, their receptors, and the signaling cascades that link to the induction of stress responses in tissues targeted by these neuronal signals.

4.2 The Physiological Significance of UPR^{mt}

Previous studies report that induction of UPR^{mt} is required for longevity associated with perturbation of mitochondrial respiration, as *ubl-5*, *haf-1* and *atfs-1*, genes required for UPR^{mt} induction, are required for lifespan extension in animals with mitochondrial inhibition (Durieux et al., 2011; Houtkooper et al., 2013; Merkwirth et al., 2016; Schieber and Chandel, 2014). The protective nature of UPR^{mt} is further supported by its importance in supporting animal development in the presence of severe mitochondrial stress (Benedetti et al., 2006) and the fact that *atfs-1* activates a wide array of genes in cellular energetics, autophagy and pathogen immunity (Nargund et al., 2015; Nargund et al., 2012; Pellegrino et al., 2014). We find that mutations of *fzo-1* trigger robust UPR^{mt}, and the mutant animals show increased



resistance to heat stress that presumably perturbs mitochondrial proteome (data not shown). The *fzo-1* mutant is slow in development and has fewer progeny, facts that are consistent with severe mitochondrial dysfunctions in this mutant. In this regard, we favor the idea that UPR^{mt} induction in the *fzo-1* mutant is a compensatory protection that serves as a preemptive measure to prime the animals for further mitochondrial stress. Consistent with this, we find that inactivation of genes required for UPR^{mt} induction severely delays the development of the *fzo-1* mutant (data not shown). Together these data implicate the UPR^{mt} as an important physiological and genetic maneuver for stress resistance.

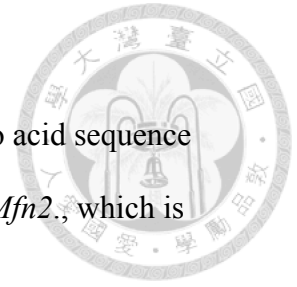
Inhibition of mitochondrial respiration triggers mitochondrial fragmentation (Haynes et al., 2007; Haynes et al., 2010). Previous studies indicate that the *fzo-1* mutant has excessive oxidative stress (Johnson and Nehrke, 2010), a hint that mitochondrial respiration is disrupted in this mutant. Consistent with this, we find that oxygen consumption is reduced in the *fzo-1* mutant. Our genetic experiments further suggest that *fzo-1* acts genetically in the mitochondrial respiratory pathway to modulate systemic homeostasis of mitochondrial proteome. Intestinal or neuronal overexpression FZO-1 partially rescued fragmented mitochondria in the *fzo-1* mutant. This is striking, as it indicates cell non-autonomous control of mitochondrial dynamics. We favor the idea that restoration of mitochondrial respiration and dynamics in the neurons will reduce stress modulators emitted from the stressed neurons, and as a consequence UPR^{mt} in distal tissues is tempered, resulting in a more connected mitochondrial morphology. Future investigations will be necessary to untangle the complex interplay between mitochondrial dynamics, stress resistance and longevity, under the remote control from the nervous system.

Chapter 5 FIGURES



Figure 1. Characterization of the *fzo-1* mutant.

(A) *fzo-1* gene structure. Black boxes are exons. (B) Alignment of amino acid sequence of the GTPase domain between *C. elegans fzo-1* and mammalian *Mfn1/Mfn2*, which is underlined green.



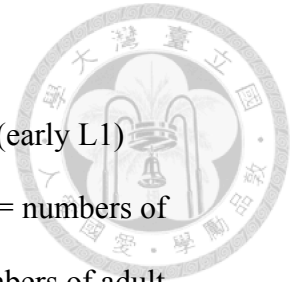
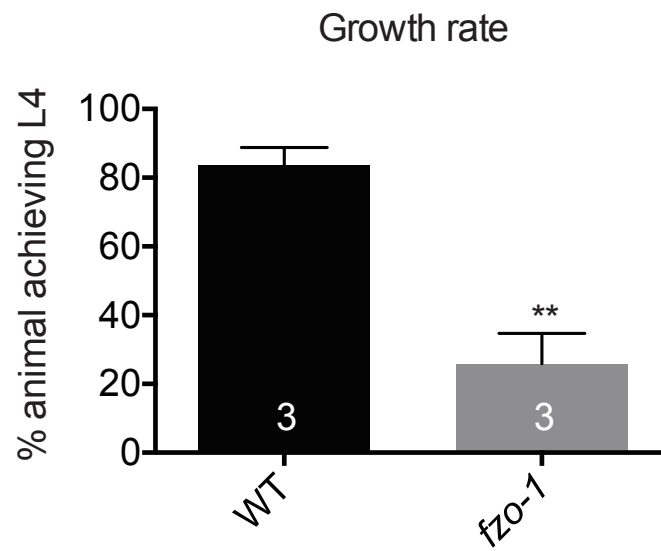


Figure 2. Pleiotropic defects in the *fzo-1* mutant.

(A) Growth rate analysis. Percentage of newly hatched wild-type larvae (early L1) reaching the last larval stage (L4) after growing for 48 hours at 20°C. N = numbers of experiments, with 50-300 animals/exp. (B) Brood size analysis. N = numbers of adult hermaphrodites analyzed. D, adult age (day). **, $p < 0.01$, unpaired t test. Error bars, S.E.M.



A



B

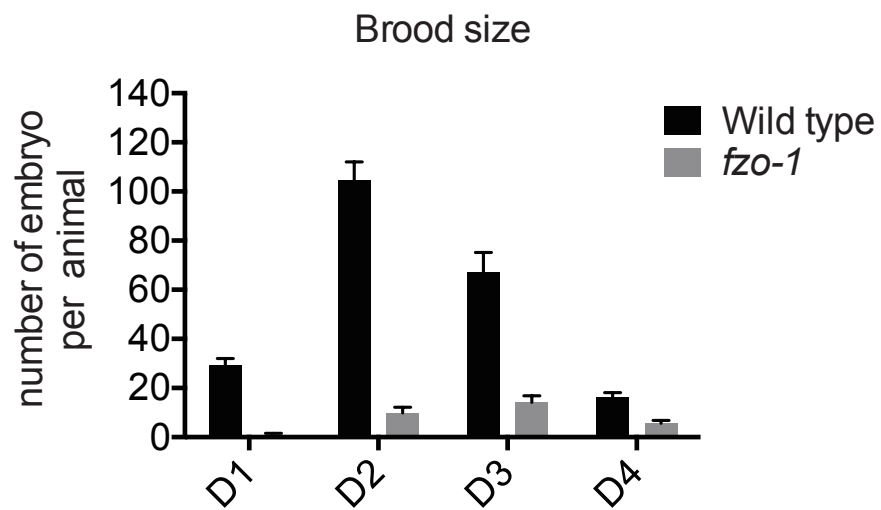
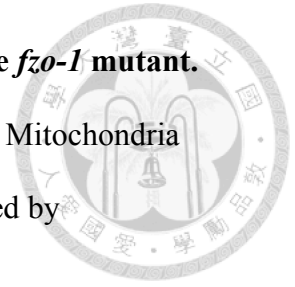


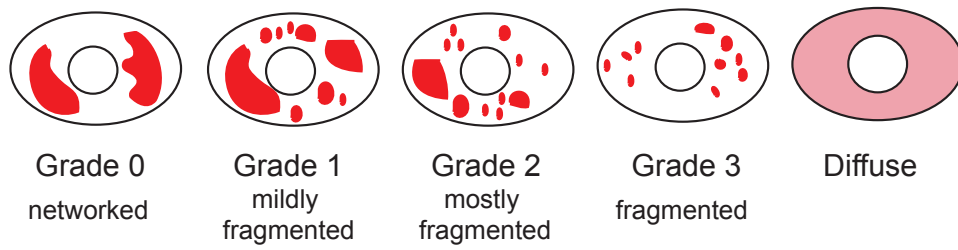
Figure 3. Mitochondria in the touch neurons were fragmented in the *fzo-1* mutant.

(A) Schematic diagrams of categories of mitochondrial morphology. (B) Mitochondria were visualized by *Pmec-7::TOMM-20::mCherry* with neurons visualized by *zdis5[Pmec-4::GFP]* in early adulthood (D1).





A



B

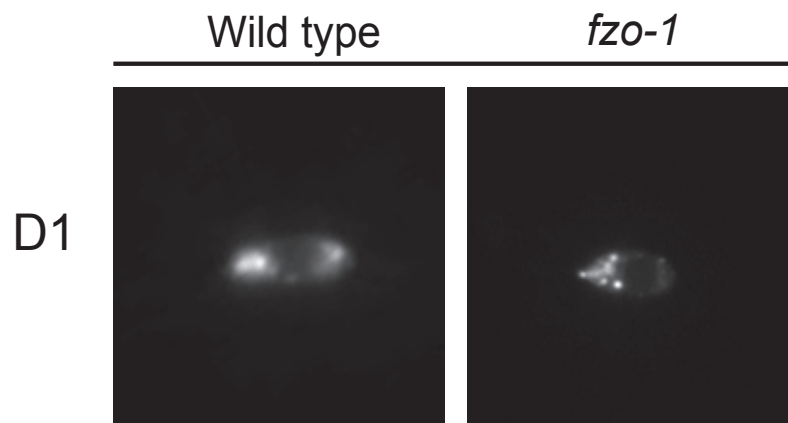
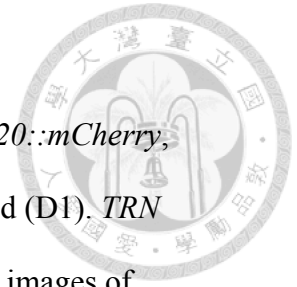


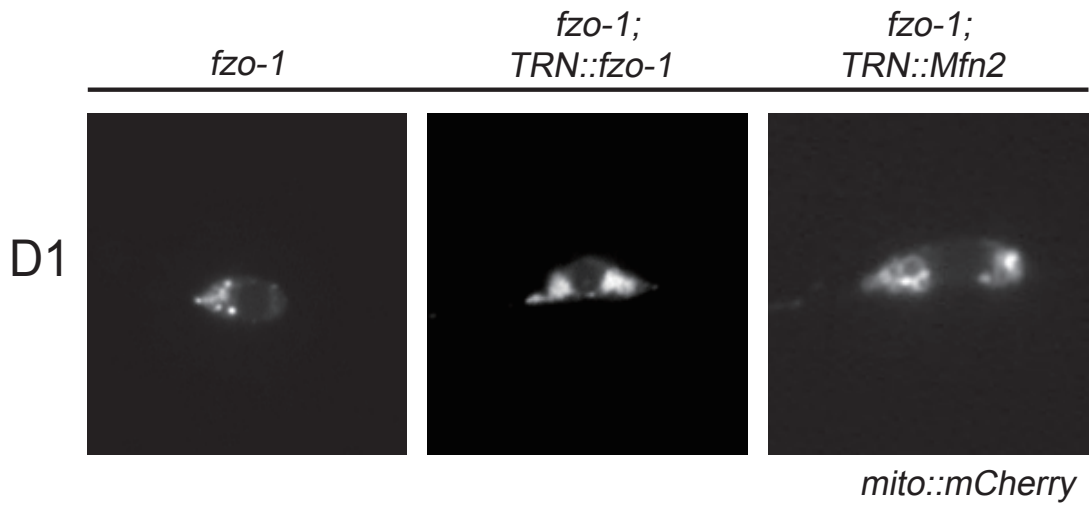
Figure 4. Mitochondrial morphology is regulated by FZO-1.

(A) Epifluorescent images of mitochondria labeled by *Pmec-7::TOMM-20::mCherry*, with touch neurons visualized by *zDIs5[Pmec-4::GFP]* in early adulthood (D1). *TRN* represents the touch neuron-specific *mec-7* promoter. (B) Epifluorescent images of GFP::FZO-1 and GFP::MFN2 expression in the touch neurons, together with *mito::mCherry*. Experiments and data were performed by Jiun-Min Hsu.





A



B

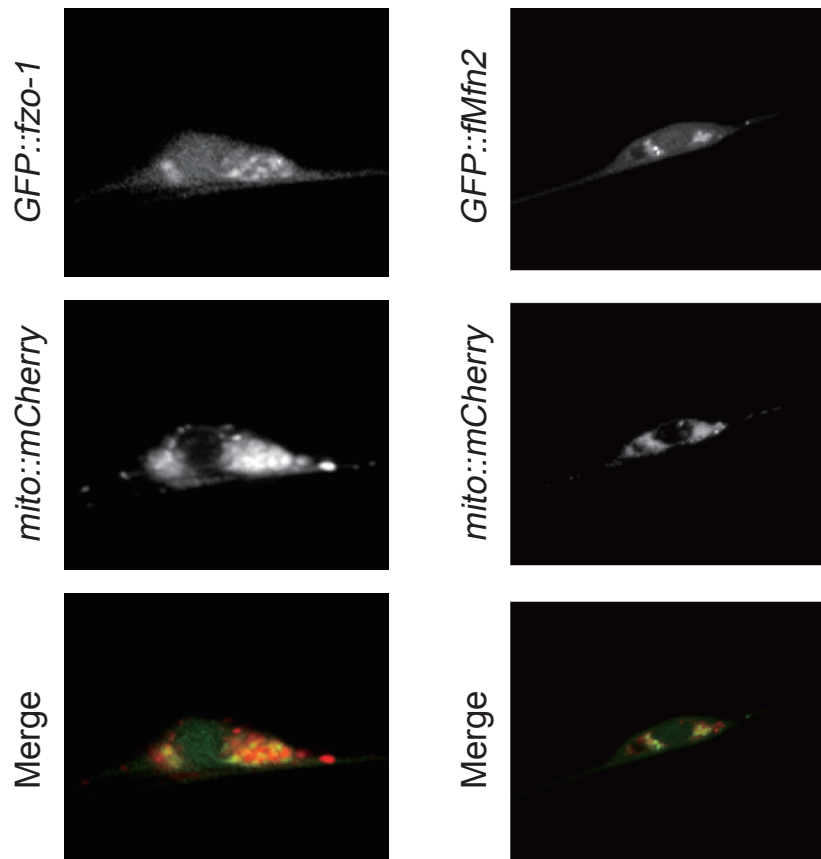
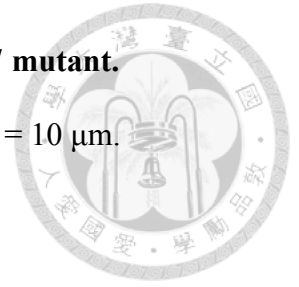


Figure 5. Mitochondria in the intestine were fragmented in the *fzo-1* mutant.

Single optical confocal section of TMRE-stained adult worms. Scale bar = 10 μ m.



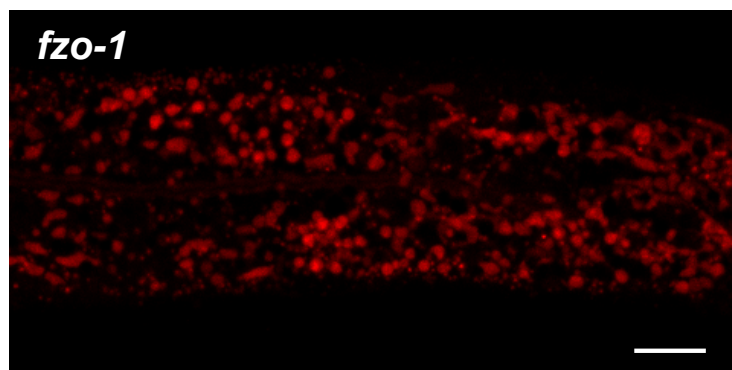
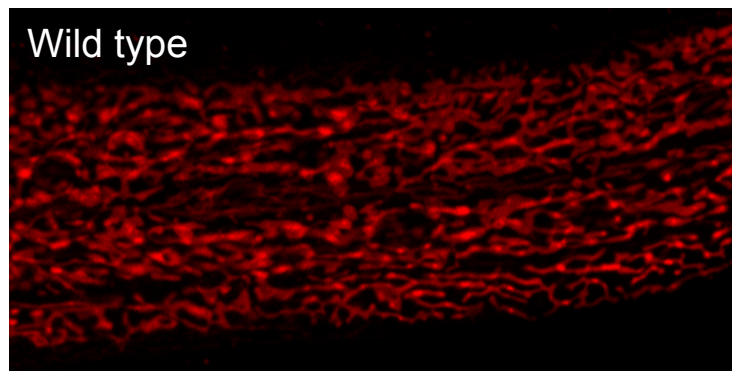
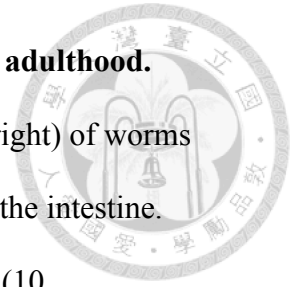


Figure 6. The *fzo-1* mutant showed robust UPR^{mt} induction in early adulthood.

(Top panel) Epifluorescent images (left) and merged DIC/GFP images (right) of worms carrying *zcls13(Phsp-6::GFP)*, and the GFP signal was most obvious in the intestine.

(Bottom panel) Quantification of *Phsp-6::GFP* pixels. Numbers are sets (10 animals/set) of animals quantified. 300 ms exposure time was used for the quantification. ***, $p < 0.001$, unpaired t test. Error bars are S.E.M.



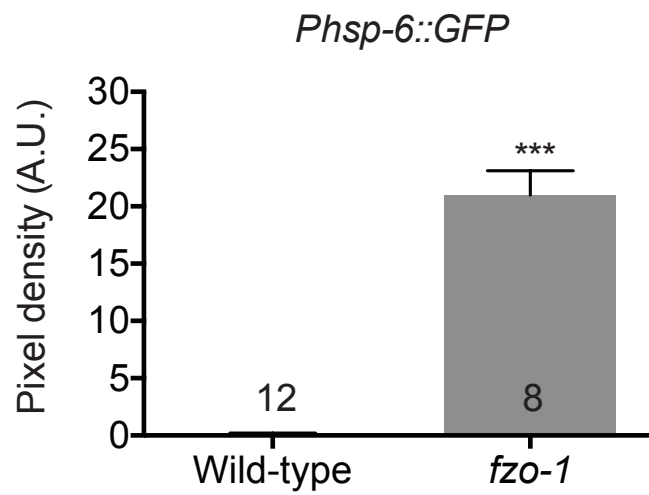
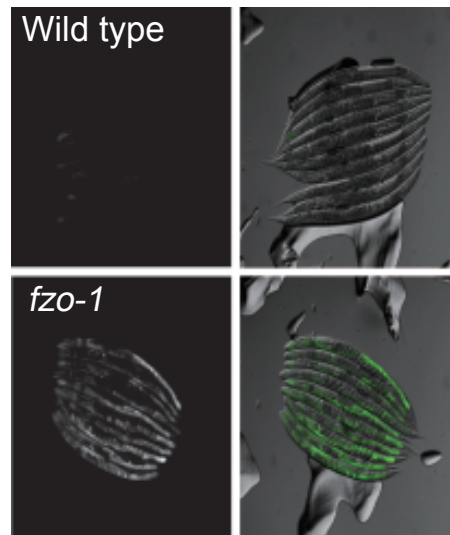
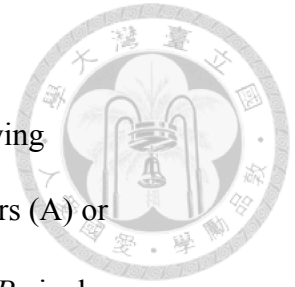


Figure 7. The *fzo-1* mutant showed intact UPR^{ER} activation.

GFP (upper panels) and merged DIC/GFP (lower panels) of worms carrying *zCIs4(Phsp-4::GFP)* UPR^{ER} reporter tested by 30°C heat shock for 6 hours (A) or dithiothreitol (DTT) treatment (B). (C, D) Quantification of *Phsp-4::GFP* pixels.

Numbers are sets (5 animals/set) of animals quantified. Error bars are S.E.M. Data were collected Jiun-Min Hsu.



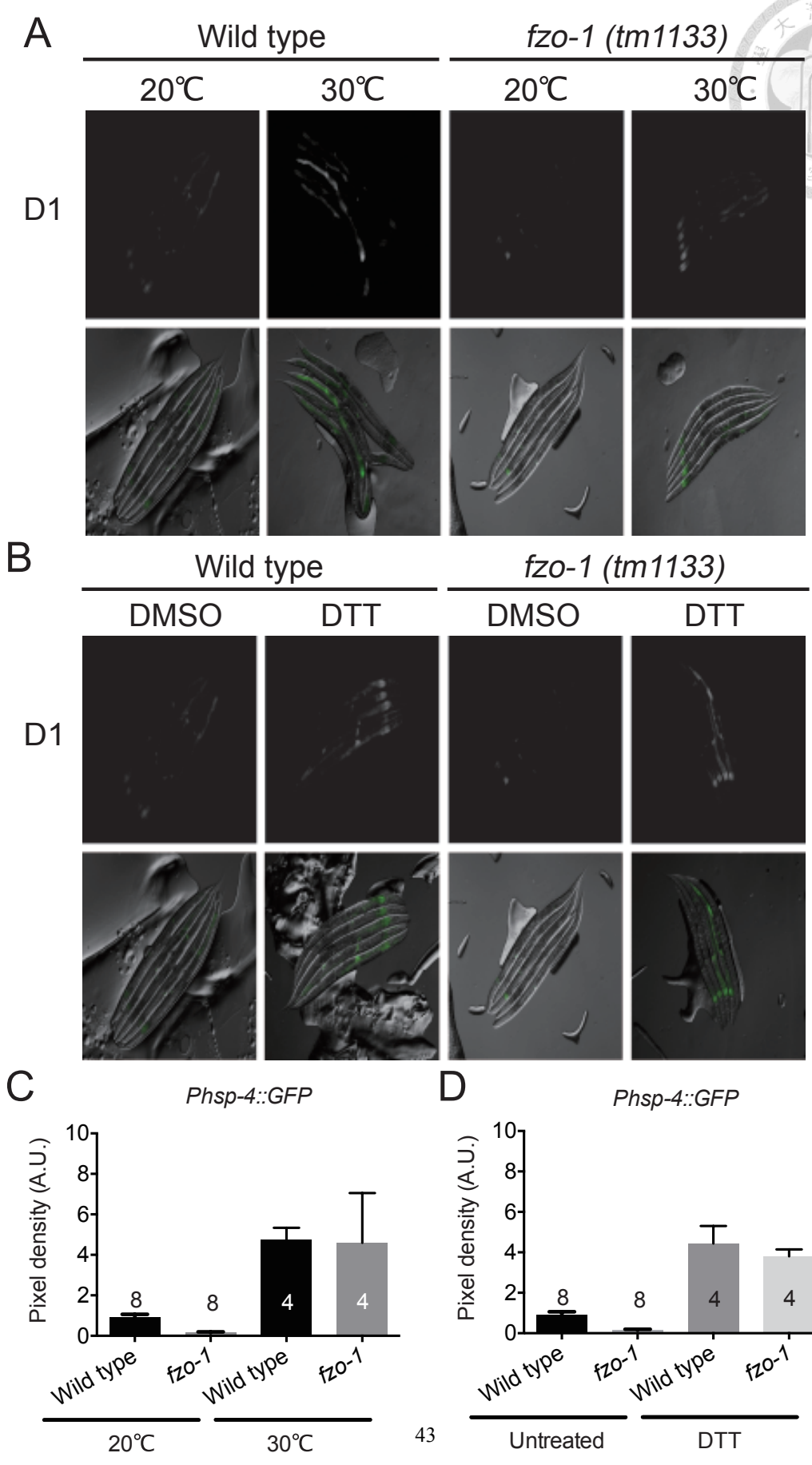


Figure 8. The *fzo-1* mutant showed intact HSR activation.

Epifluorescence images (upper) and quantification (lower) for *Phsp-16.2::GFP* HSR reporter of worms incubated at 34°C for 6 hours. Numbers are sets (5 animals/set) of animals quantified. Error bars are S.E.M.



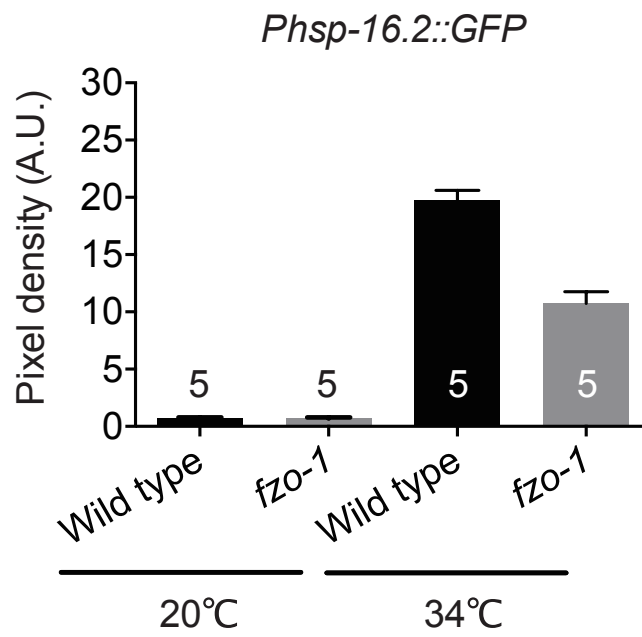
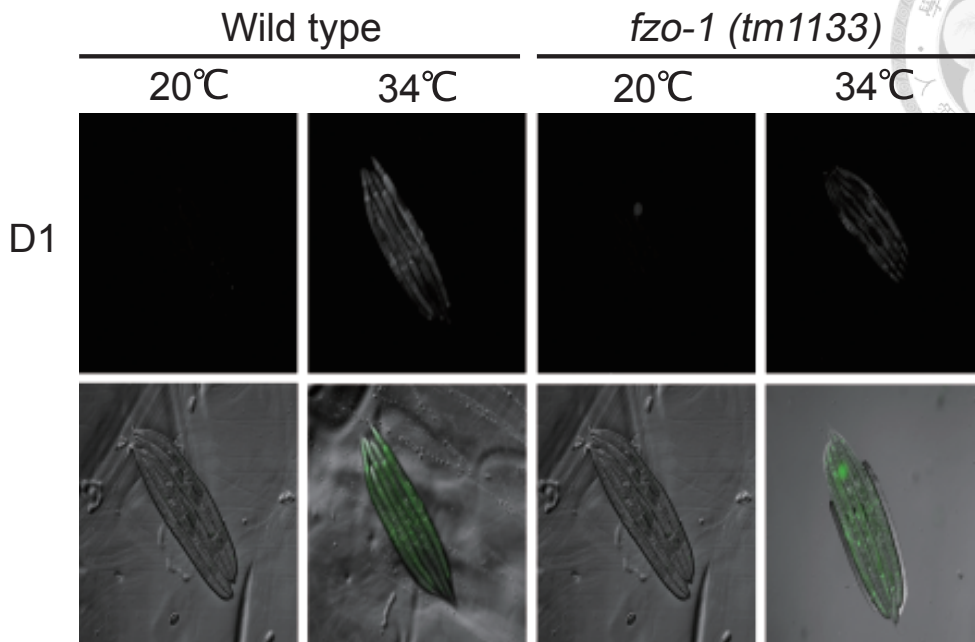
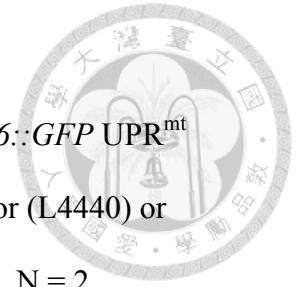


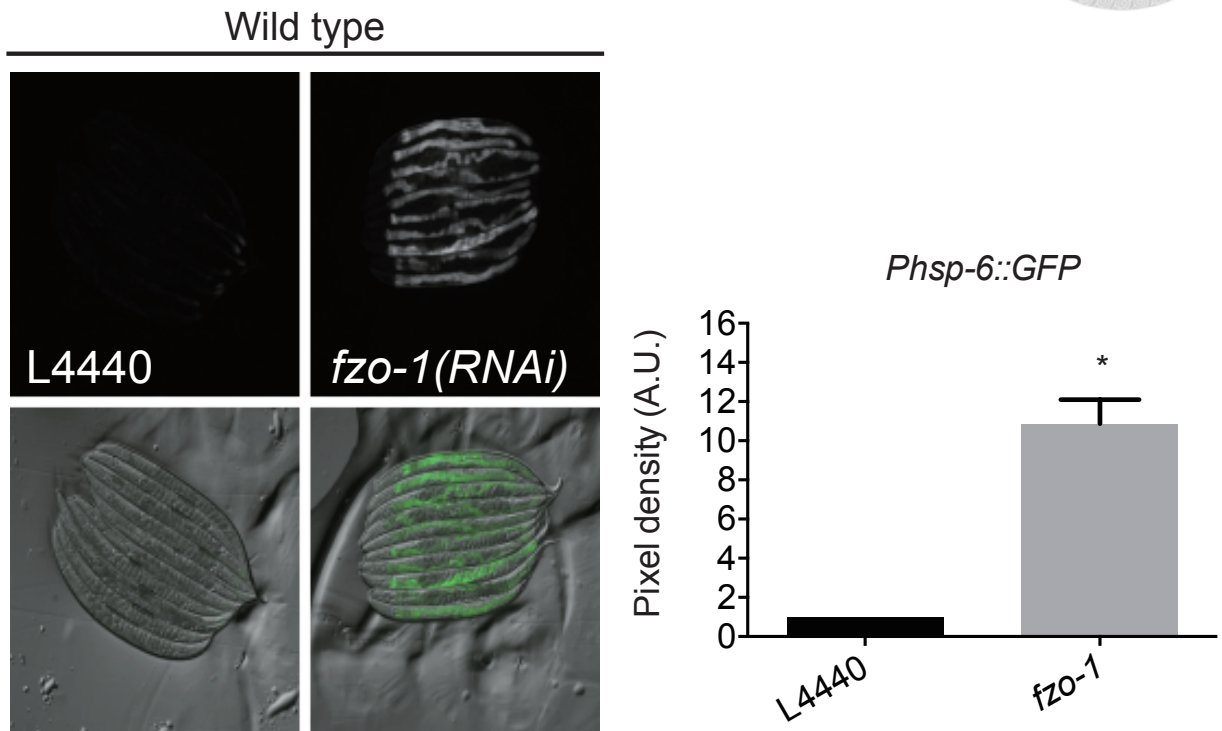
Figure 9. *fzo-1* knockdown induced maladapted UPR^{mt}.

(A) Epifluorescence images (left) and quantification (right) of the *Phsp-6::GFP* UPR^{mt} reporter in wild-type animal treated with bacteria containing empty vector (L4440) or *fzo-1* RNAi construct. Data are normalized to those of the L4440 control. N = 2 experiments, with 20-70 animals/exp. 150 ms exposure time was used for the quantification. (B) Growth rate analysis. Percentage of newly-hatched larvae (early L1) reaching the last larval stage (L4) after growing for 54 hours at 20°C on L4440 or *fzo-1* RNAi-containing bacteria. N = 3 experiments, with 35-200 animals/exp. *, $p < 0.05$, **, $p < 0.01$, unpaired *t* test. Error bars are S.E.M.





A



B

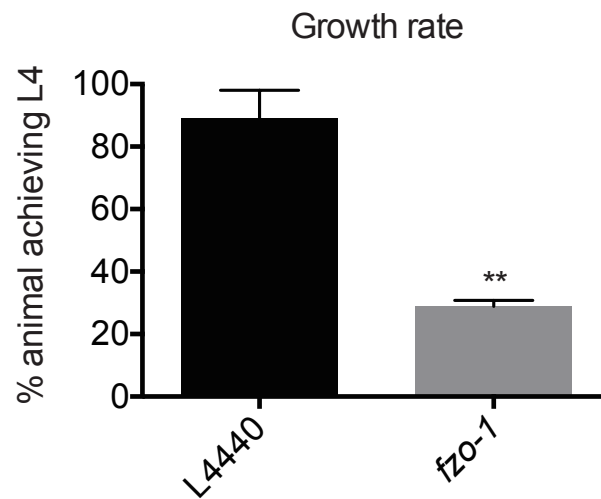


Figure 10. *hsp-6* transcripts were increased in somatic tissues of the *fzo-1* mutant.

hsp-6 transcripts detected by smFISH at third larval stage (L3). Samples are counter-stained with DAPI (blue) with *hsp-6* mRNA pseudocolored in gray.



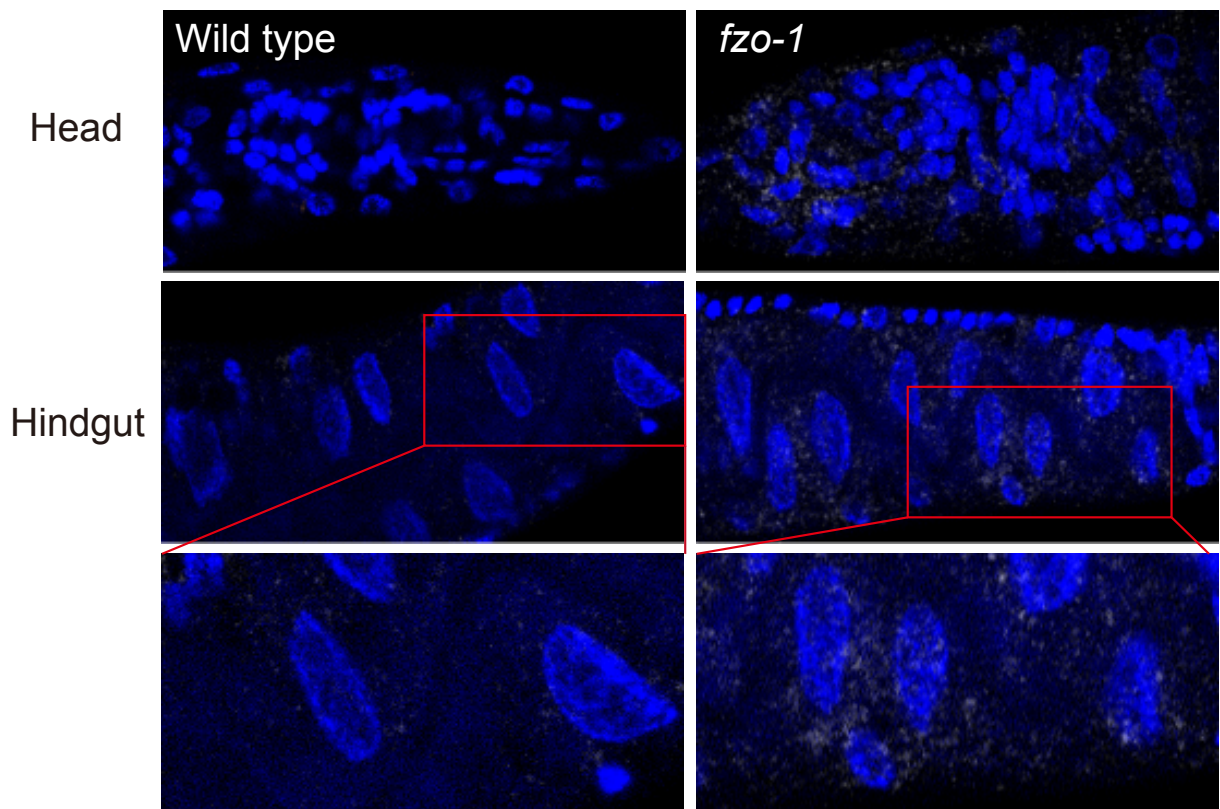


Figure 11. The *fzo-1* mutant showed increased *hsp-60* expression.

Epifluorescence or DIC/GFP merged images (upper) and quantification (lower) of the *zCIs9(Phsp-60::GFP)* reporter. Numbers are sets (5-10 animals/set) of animals quantified. 500 ms exposure time was used for the quantification. Error bars are S.E.M.



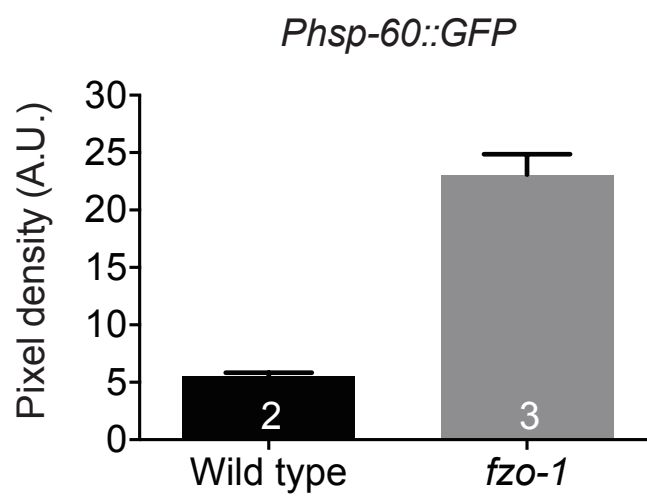
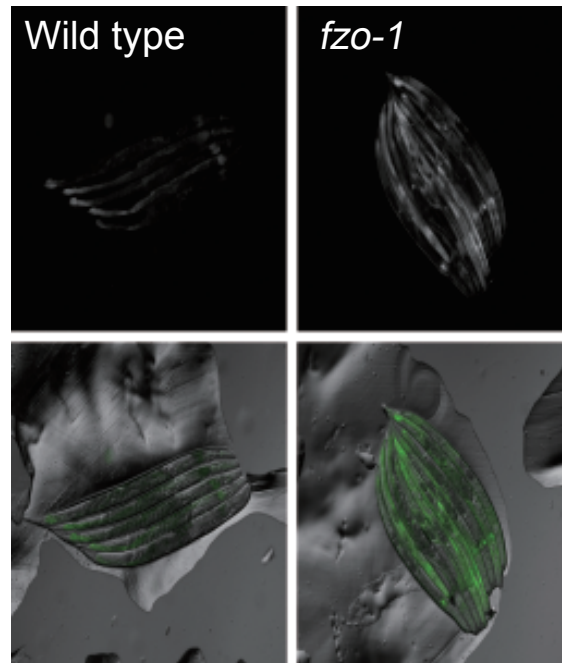
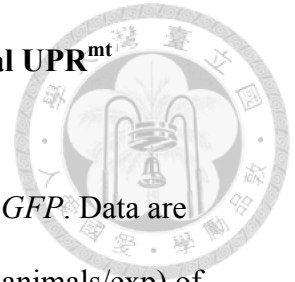


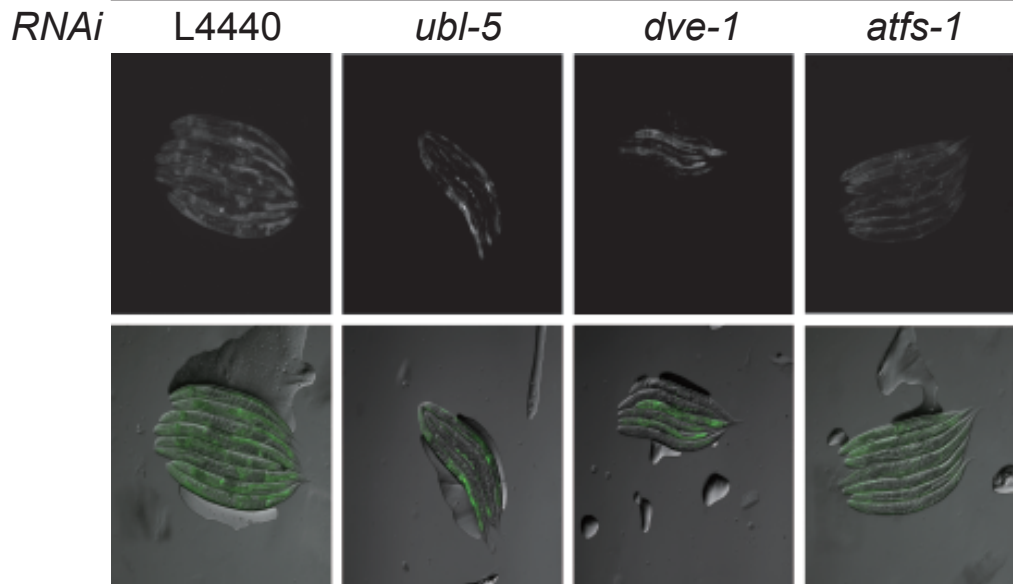
Figure 12. Maladapted UPR^{mt} in the *fzo-1* mutant requires canonical UPR^{mt} genes.

Epifluorescence images (upper) and quantification (bottom) for *Phsp-6::GFP*. Data are normalized to the empty vector control (L4440). Numbers are sets (6-40 animals/exp) of experiments. *, $p < 0.05$, ***, $p < 0.001$, unpaired t test. Error bars are S.E.M.





fzo-1(tm1133)



Phsp-6::GFP

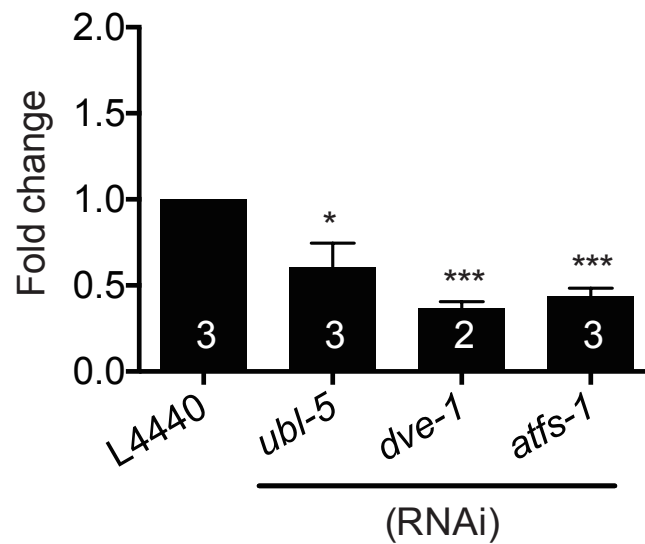
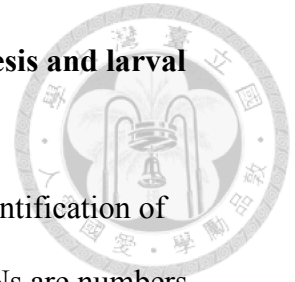


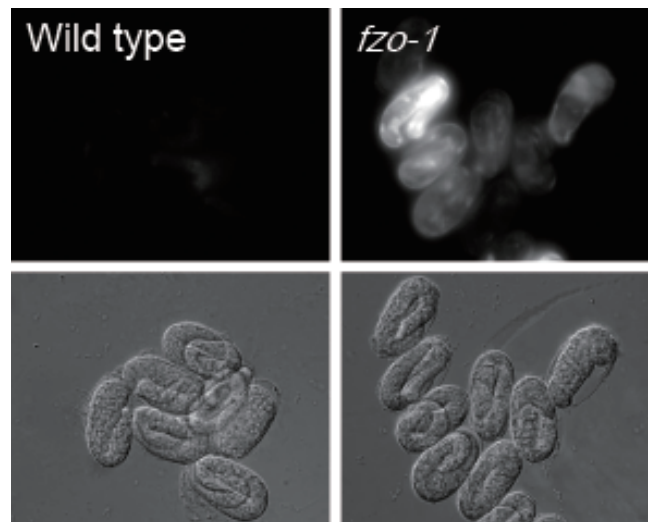
Figure 13. UPR^{mt} is constitutively activated throughout embryogenesis and larval development in the *fzo-1* mutant.

(A) Epifluorescent images of *Phsp-6::GFP*-containing embryos (B) Quantification of *Phsp-6::GFP* pixels of L3 and L4 larvae as well as young adult animals. Ns are numbers of experiments. Error bars are S.E.M.





A



B

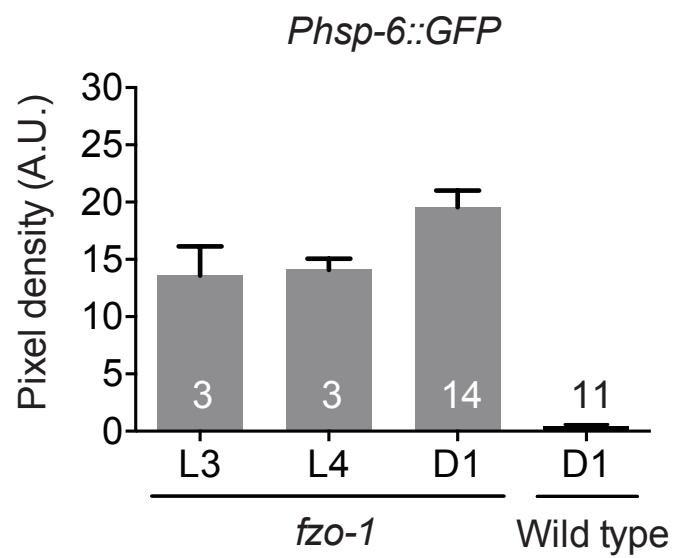
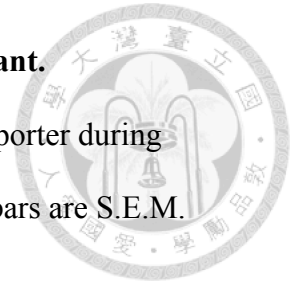


Figure 14. UPR^{mt} activation persisted during aging in the *fzo-1* mutant.

(A) Epifluorescent images and (B) quantification of the *Phsp-6::GFP* reporter during aging. Numbers are sets (5-10 animals/set) of animals quantified. Error bars are S.E.M.



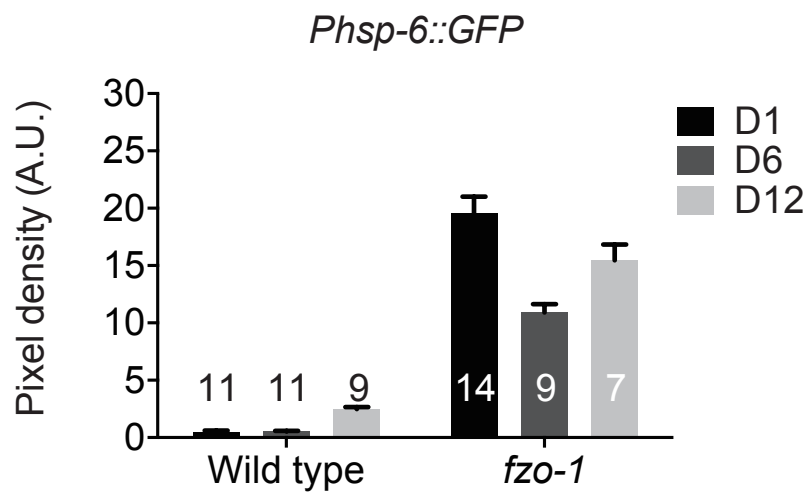
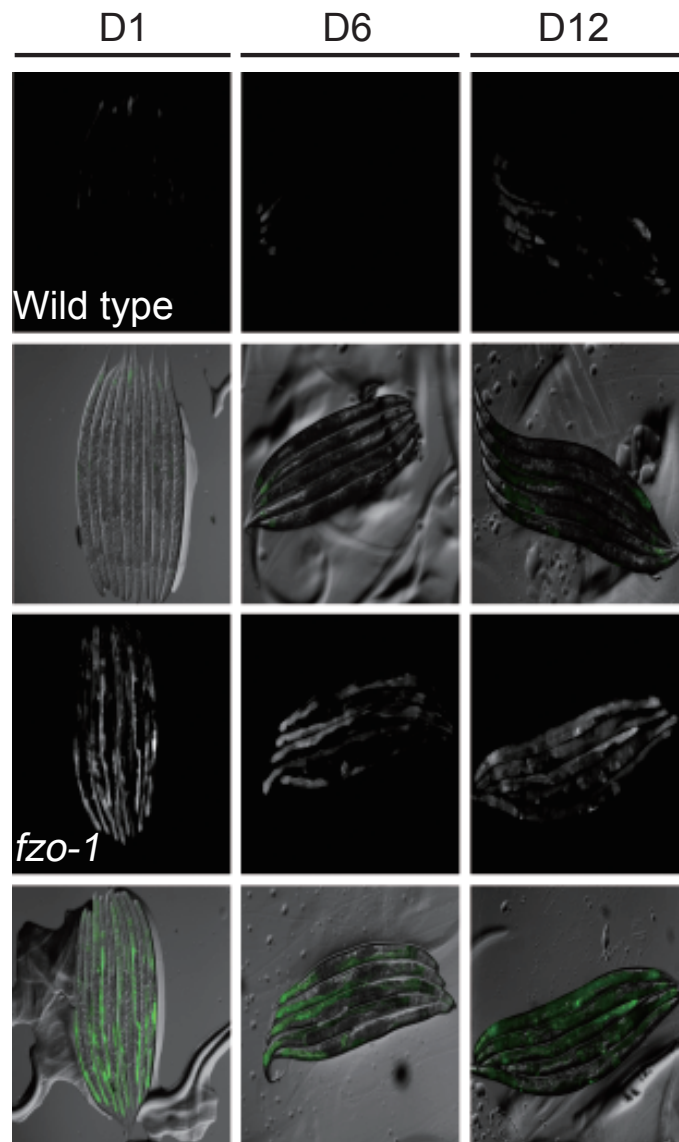
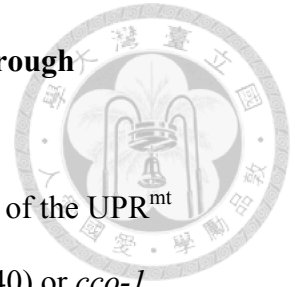


Figure 15. *fzo-1* mutation may induce maladapted UPR^{mt} in part through respiratory inhibition.

Epifluorescence images (upper panels) and quantification (lower panels) of the UPR^{mt} reporter in wild-type or the *fzo-1* mutant treated with empty vector (L4440) or *cco-1* RNAi. Data are normalized to that of wild-type animals treated with with empty vector (L4440). N = 3 experiments, 8-50 animals/exp. ***, $p < 0.001$, unpaired t test. Error bars, S.E.M.



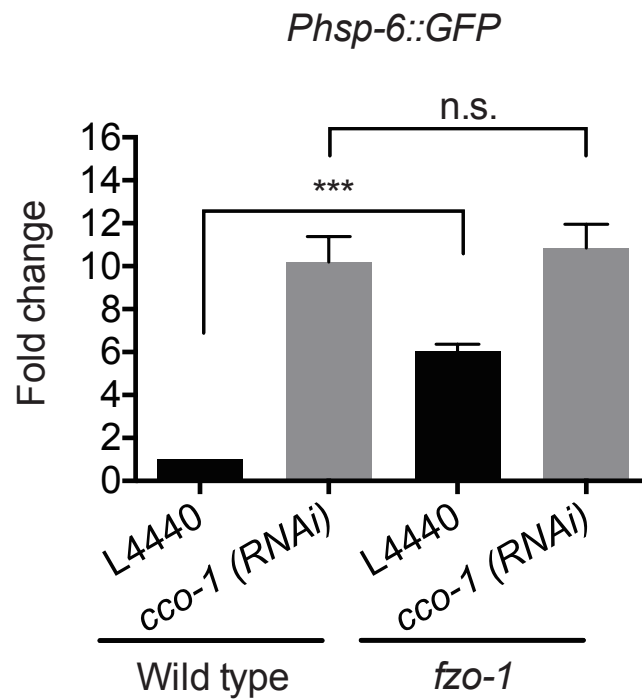
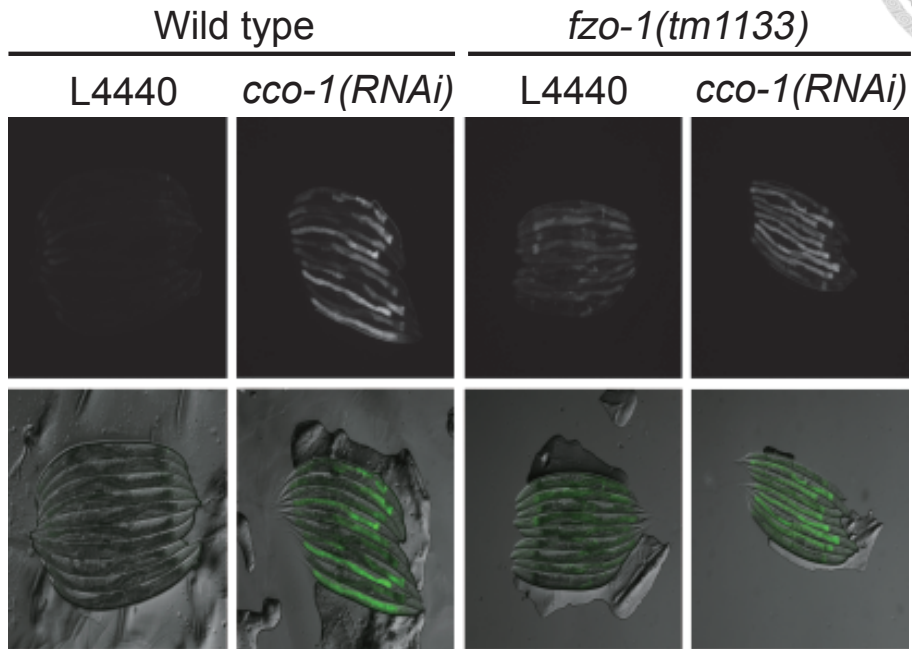


Figure 16. Mitochondrial dynamics influenced respiration.

Quantification of oxygen consumption in early adulthood. Error bars, S.E.M.



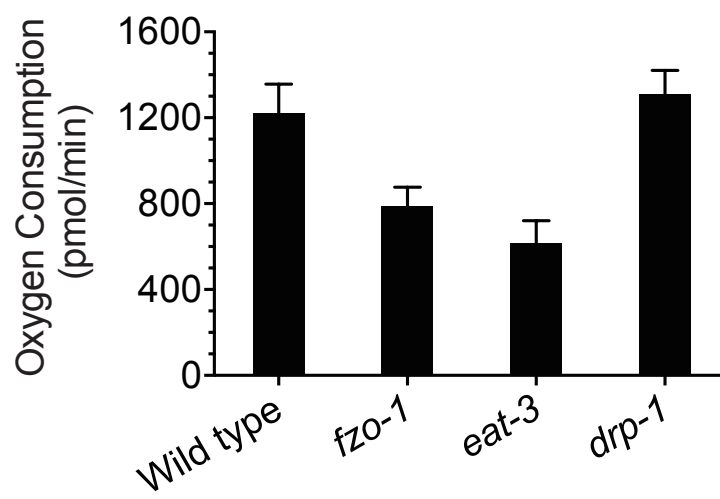
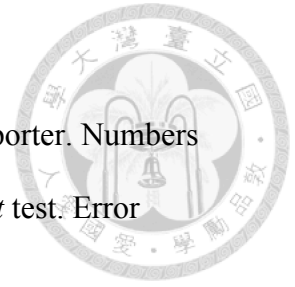


Figure 17. Mitochondrial dynamics controlled UPR^{mt} activation.

Epifluorescence images (upper) and quantification (lower) for UPR^{mt} reporter. Numbers are sets (10 animals/set) of animals quantified. ***, $p < 0.001$, unpaired t test. Error bars, S.E.M.



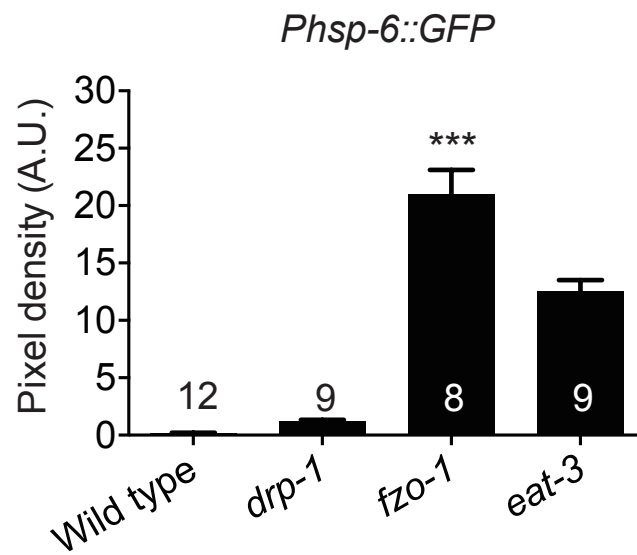
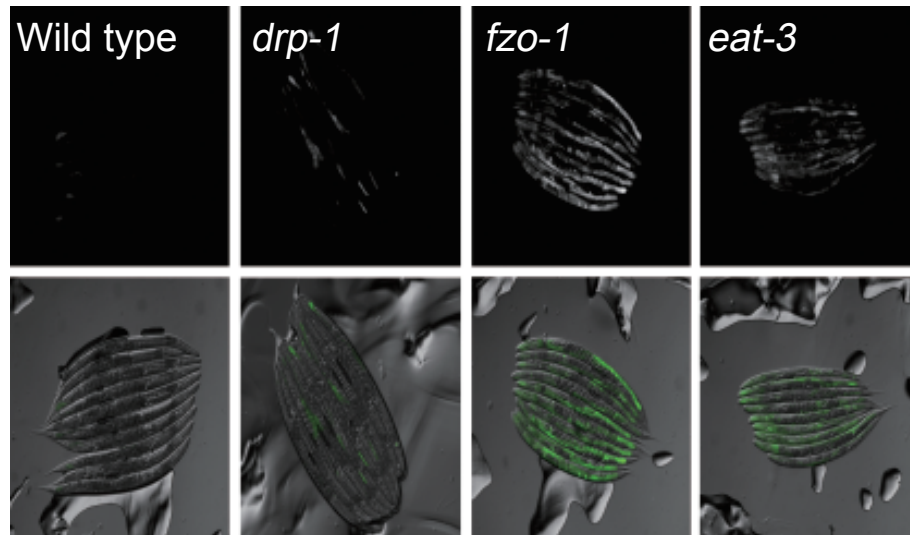


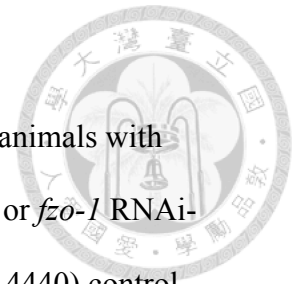
Figure 18. Intestine-specific *fzo-1* knockdown triggered UPR^{mt}.

(A) Epifluorescence images (left) and quantification (right) of UPR^{mt} in animals with intestine-specific sensitivity to RNAi treated with empty vector (L4440) or *fzo-1* RNAi-containing bacteria. Data are normalized to that with the empty vector (L4440) control.

Numbers are sets (50-55 animals/exp) of experiments quantified. 150 ms exposure time

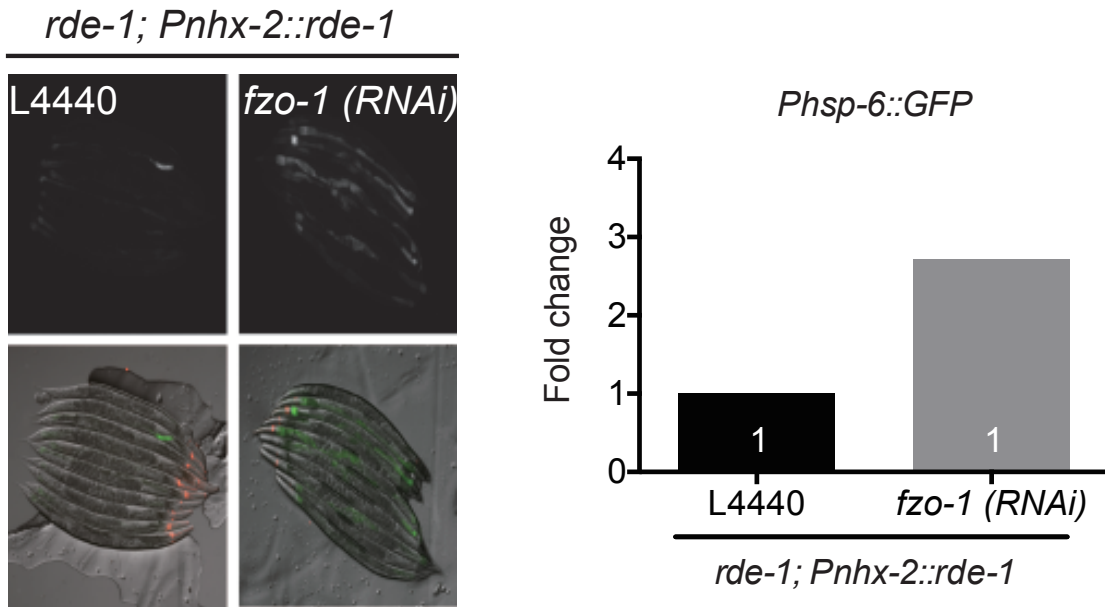
was used for quantification. (B) Single confocal optical section of TMRE-stained

worms showing the morphology of intestinal mitochondria Scale bar = 10 μm .





A



B

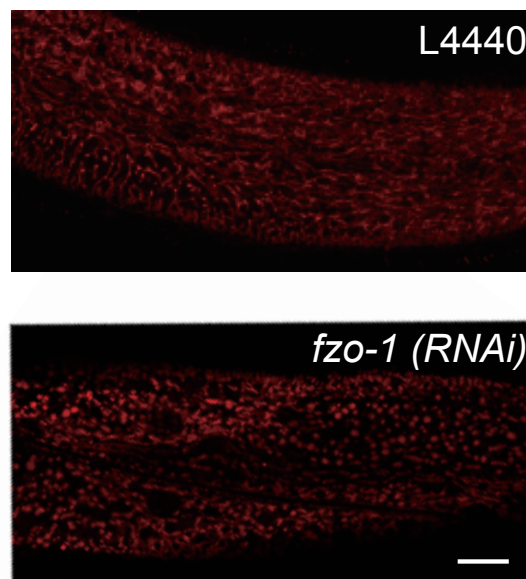
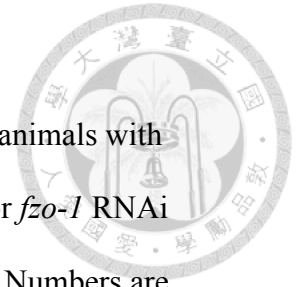


Figure 19. Muscle-specific *fzo-1* knockdown did not induce UPR^{mt}.

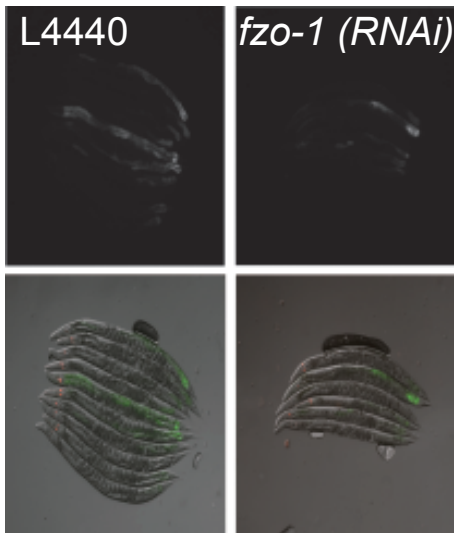
(A) Epifluorescence images (left) and quantification (right) of UPR^{mt} in animals with muscle-specific sensitivity to RNAi treated with empty vector (L4440) or *fzo-1* RNAi bacteria. Data are normalized to that with empty vector (L4440) control. Numbers are sets (20 animals/exp) of experiments quantified. 150 ms exposure time was used for quantification. (B) Single confocal optical section of TMRE-stained worms showing the morphology of muscle and some intestinal mitochondria. Scale bar = 10 μm .



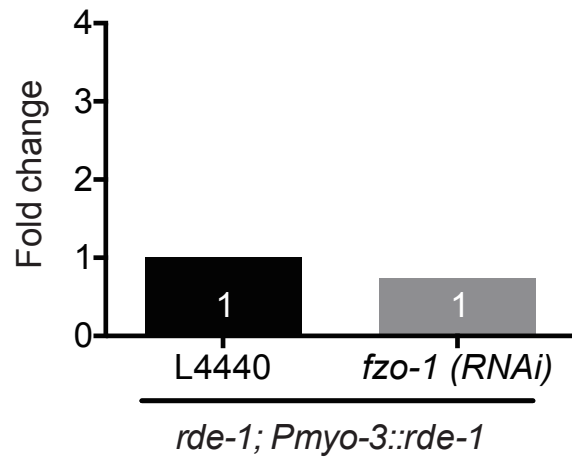


A

rde-1; Pmyo-3::rde-1



Phsp-6::GFP



B

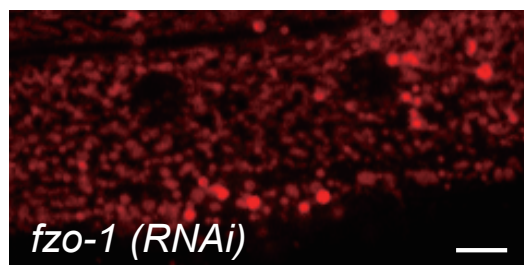
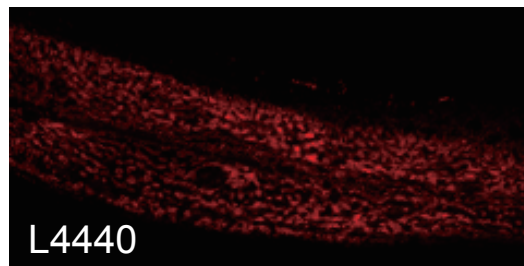
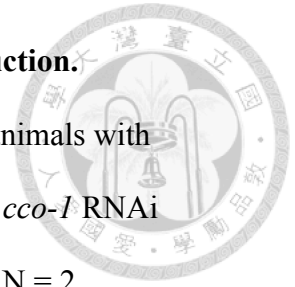


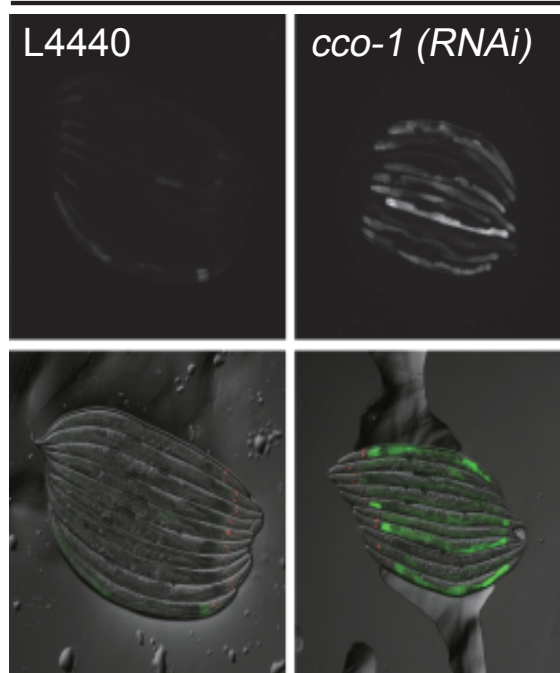
Figure 20. Intestine-specific *cco-1* knockdown triggered UPR^{mt} induction.

Epifluorescence images (upper) and quantification (lower) of UPR^{mt} in animals with intestine-specific RNAi sensitivity treated with empty vector (L4440) or *cco-1* RNAi bacteria. Data are normalized to that with empty vector (L4440) control. N = 2 experiments, 30-40 animals/exp. *, $p < 0.05$, unpaired t test. 100 ms exposure time was used for quantification.





rde-1; Pnhx-2::RDE-1



Phsp-6::GFP

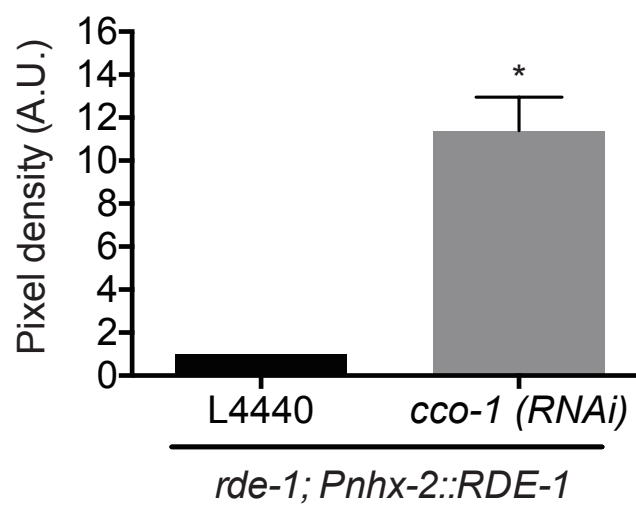
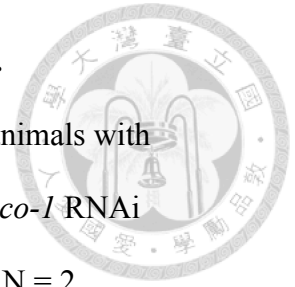


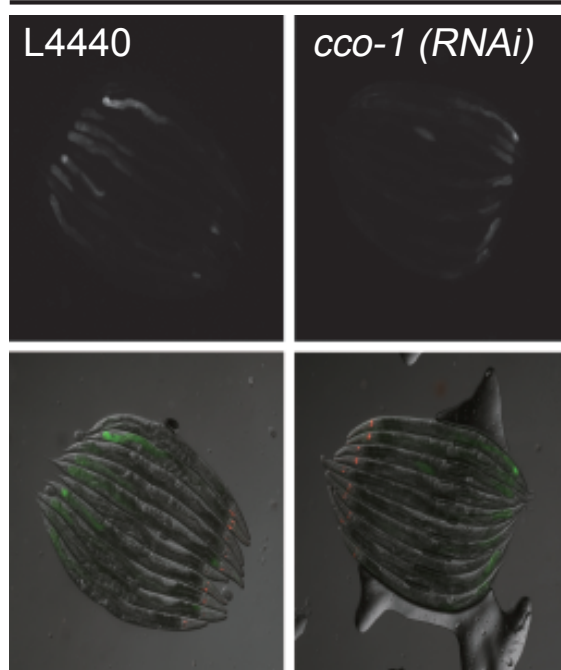
Figure 21. Muscle-specific *cco-1* knockdown failed to induce UPR^{mt}.

Epifluorescence images (upper) and quantification (lower) of UPR^{mt} in animals with muscle-specific RNAi sensitivity treated with empty vector (L4440) or *cco-1* RNAi bacteria. Data are normalized to that with empty vector (L4440) control. N = 2 experiments, 30-40 animals/exp. unpaired *t* test. 100 ms exposure time was used for quantification.





rde-1; Pmyo-3::RDE-1



Phsp-6::GFP

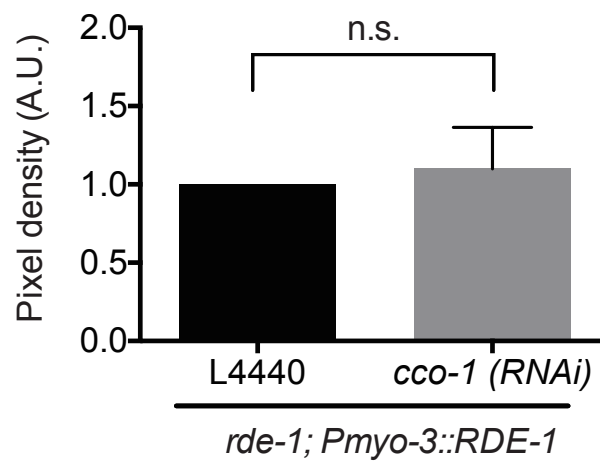


Figure 22. Neuron-specific *fzo-1* knockdown triggered UPR^{mt}.

Epifluorescence images (upper) and quantification (lower) of UPR^{mt} in transgenic animals expressing *Punc-119::dsfzo-1(RNAi)* extrachromosome array. Data are normalized to sibling animals that lose the array. N = 3 experiments, 28-50 animals/exp. ***, $p < 0.001$, unpaired *t* test. Error bars, S.E.M. 150 ms exposure time was used for quantification.



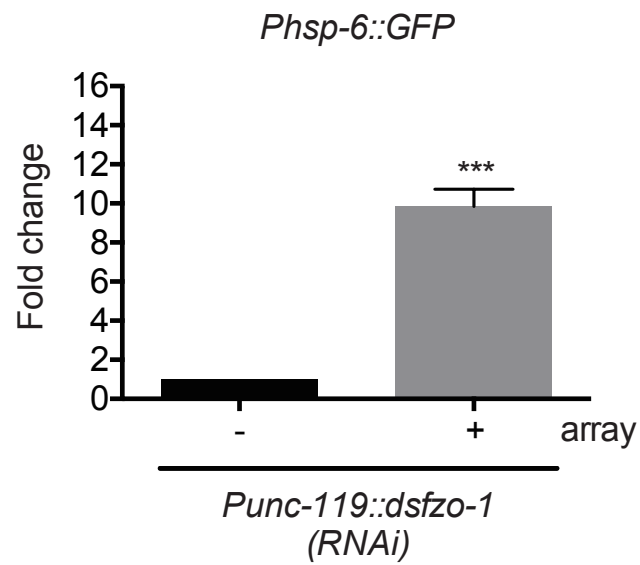
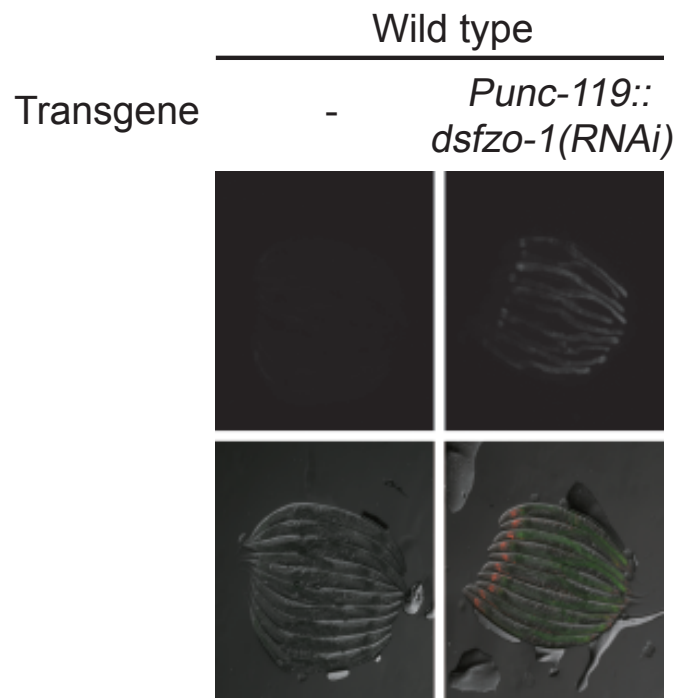


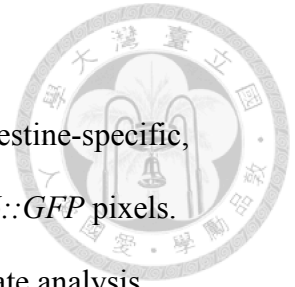
Figure 23. Tissue-specific *fzo-1* expression and the rescue of UPR^{mt}.

(A) Epifluorescent images of *fzo-1* animals expressing *fzo-1* from the intestine-specific, neuron-specific or the 3 kb *fzo-1* promoters. (B) quantification of *Phsp-6::GFP* pixels.

Numbers are sets (5-10 animals/set) of animals quantified. (C) Growth rate analysis.

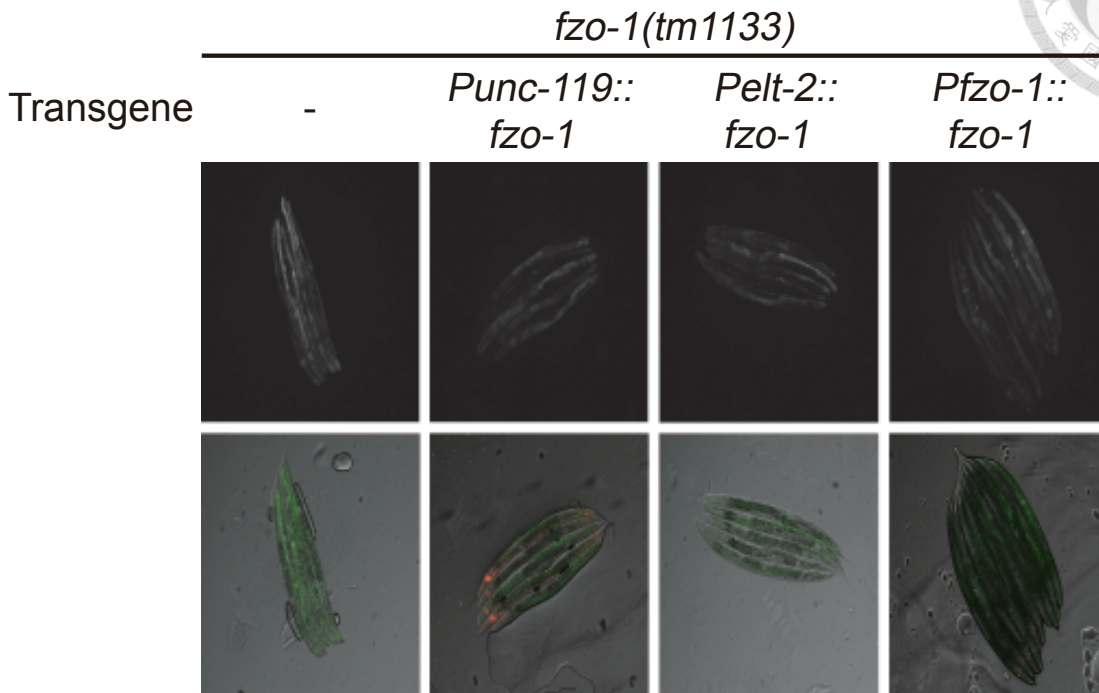
Percentage of newly-hatched larvae (early L1) reaching the last larval stage (L4) after growing for 54 hours at 20°C. N = numbers of experiments, 35-200 animals/exp. ***, p

< 0.001, unpaired t test. Error bars, S.E.M.

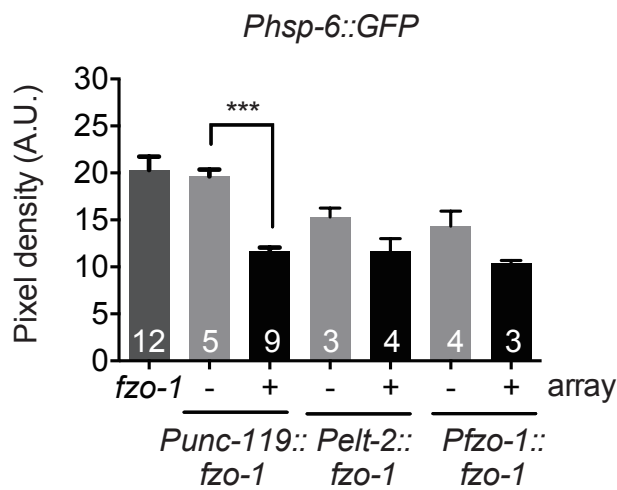




A



B



C

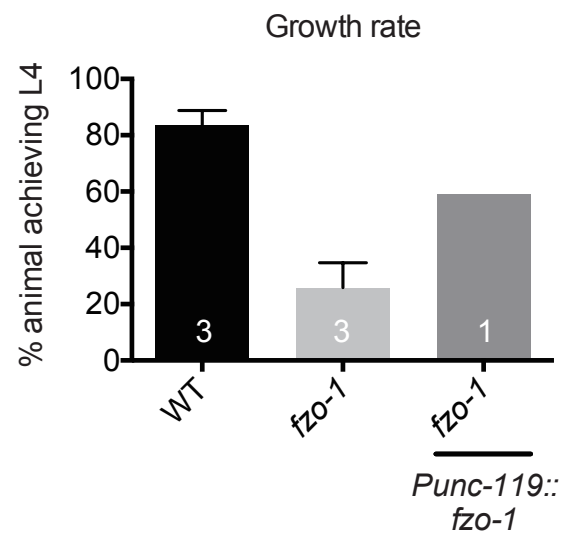


Figure 24. Intestinal mitochondrial fragmentation were partially rescued by tissue-specific FZO-1 expression.

Single optical confocal section of TMRE-stained worms. Scale bar = 10 μ m.



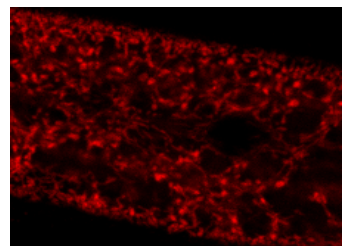
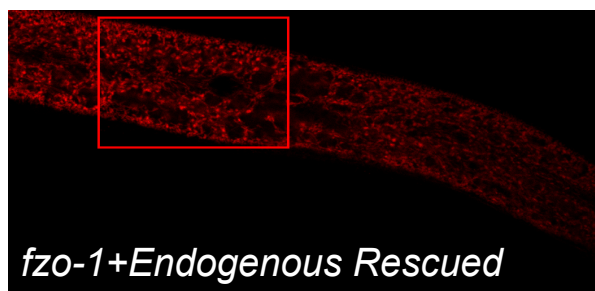
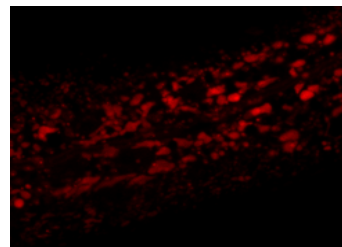
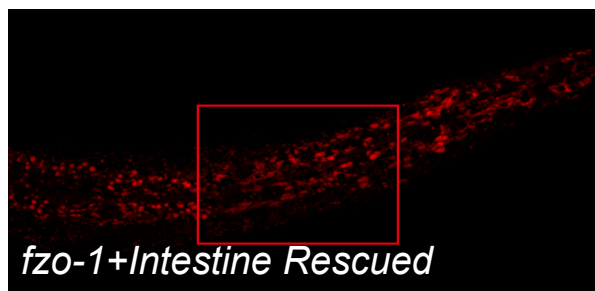
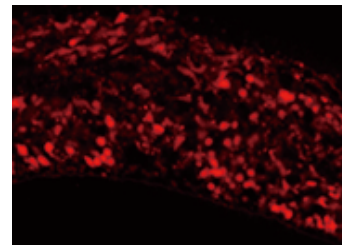
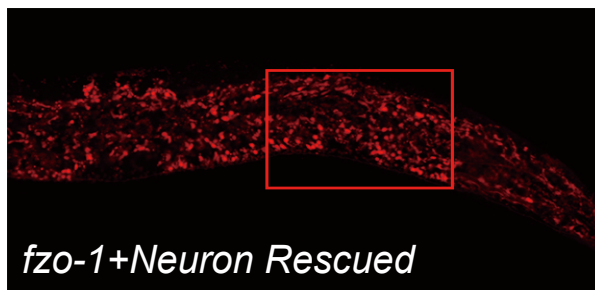
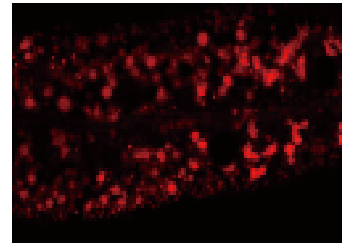
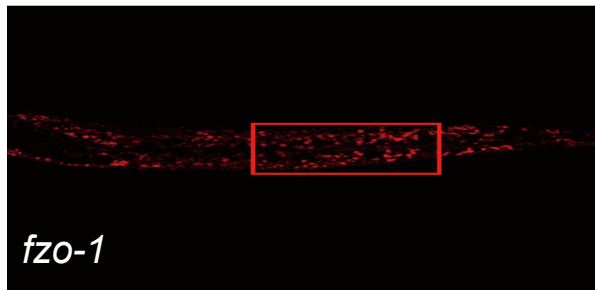


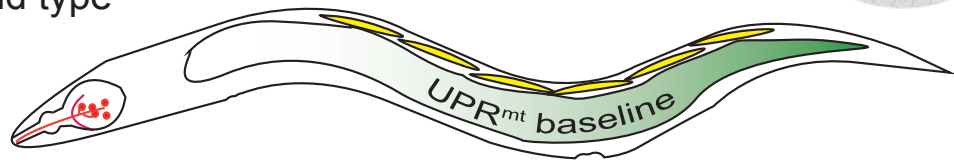
Figure 25. Models of autonomous and non-autonomous UPR^{mt} control by FZO-1.



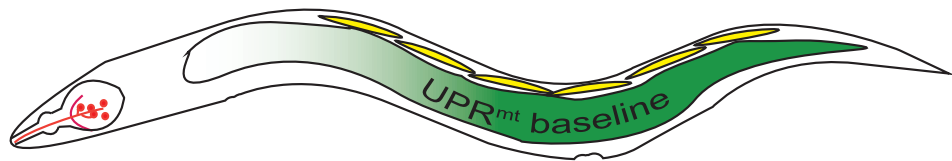


A

Wild type



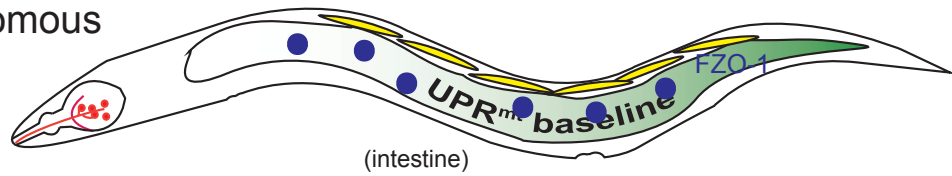
fzo-1 (*tm1133*)



B

fzo-1+ Intestinal FZO-1

Autonomous



fzo-1+ Neuronal FZO-1

Non-Autonomous

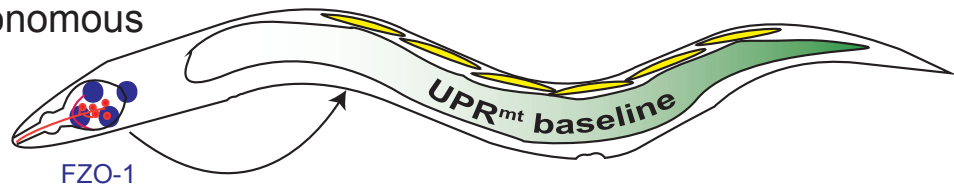


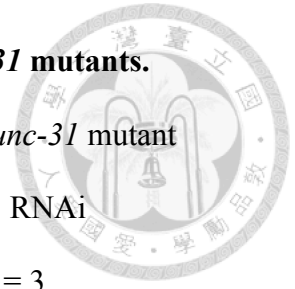
Figure 26. *cco-1* knockdown induced UPR^{mt} in the *unc-13* and *unc-31* mutants.

Epifluorescence images (left) and quantification (right) of UPR^{mt} in the *unc-31* mutant

(A) or the *unc-13* mutant (B) treated with empty vector (L4440) or *cco-1* RNAi

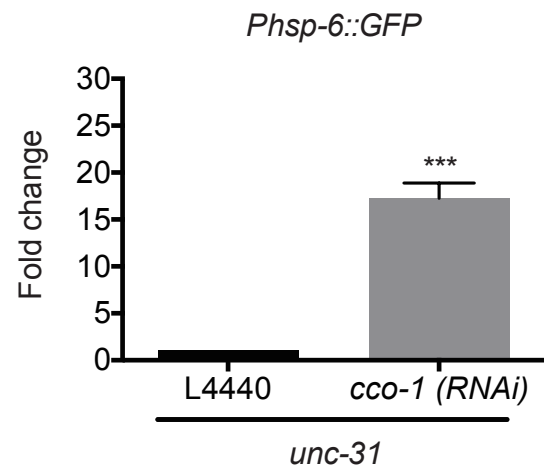
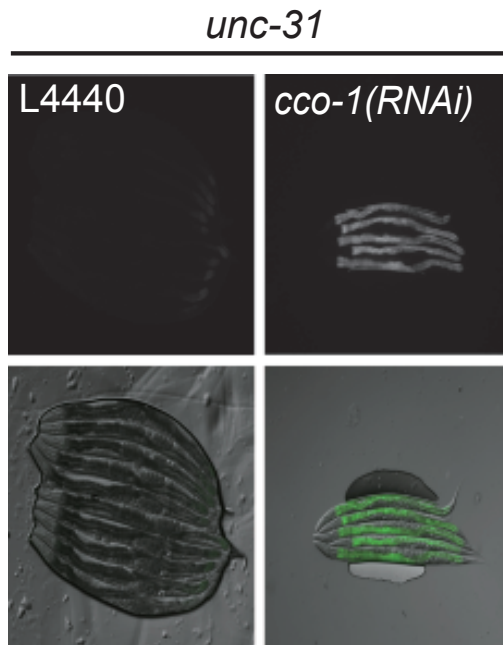
bacteria. Data are normalized to that of empty vector (L4440) control. N = 3

experiments, 8-50 animals/exp. ***, $p < 0.001$, unpaired t test. Error bars, S.E.M.





A



B

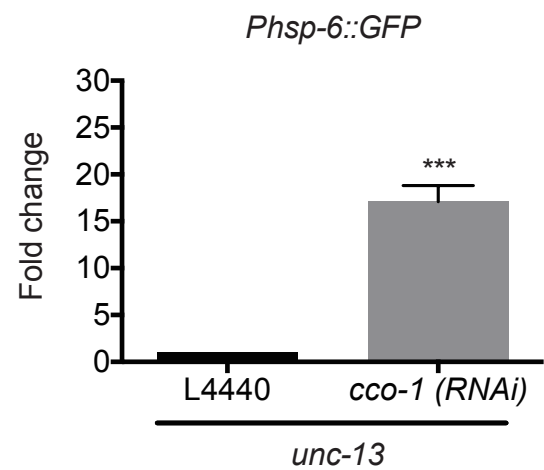
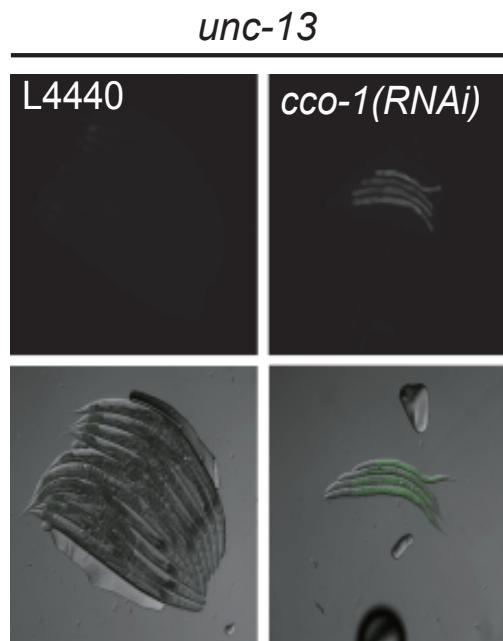


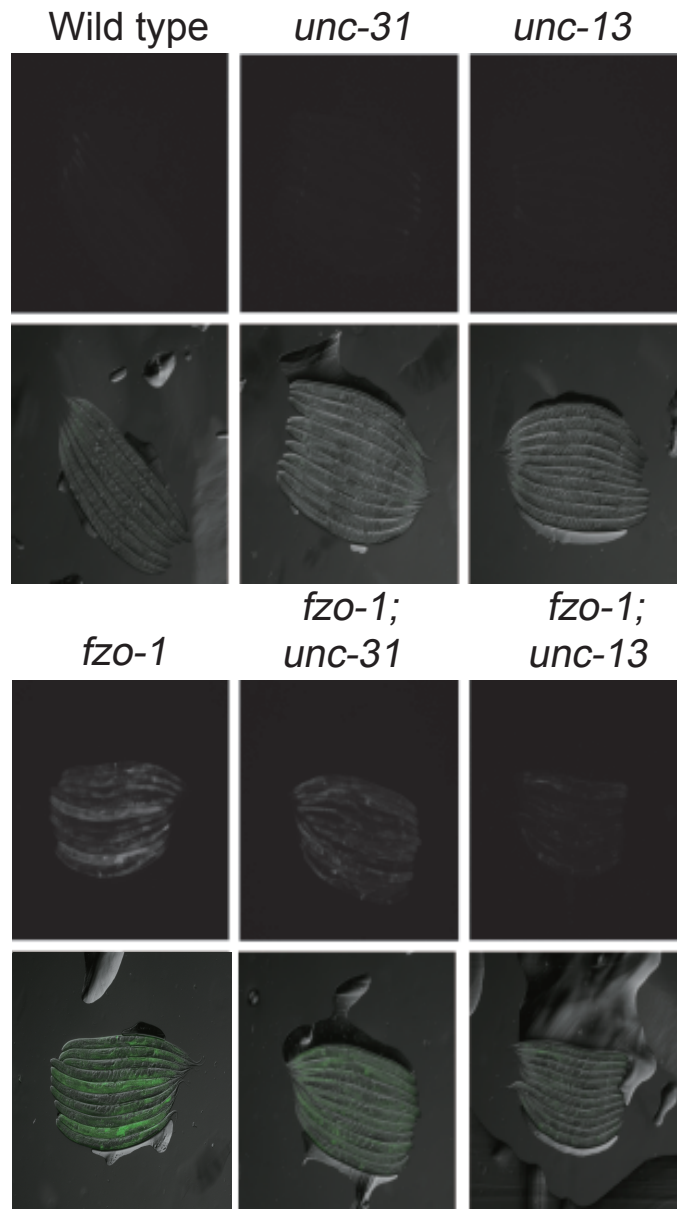
Figure 27. Cell non-autonomous induction of UPR^{mt} requires both neurotransmitters and neuropeptides.

Epifluorescence images (upper) and quantification (lower) of UPR^{mt} in animals of indicated genotypes at day1 of adulthood. Data are normalized to that of the wild type.

N = 3 experiments, 21-70 animals/exp. **, $p < 0.01$, ***, $p < 0.001$, unpaired t test.

Error bars, S.E.M.





Phsp-6::GFP

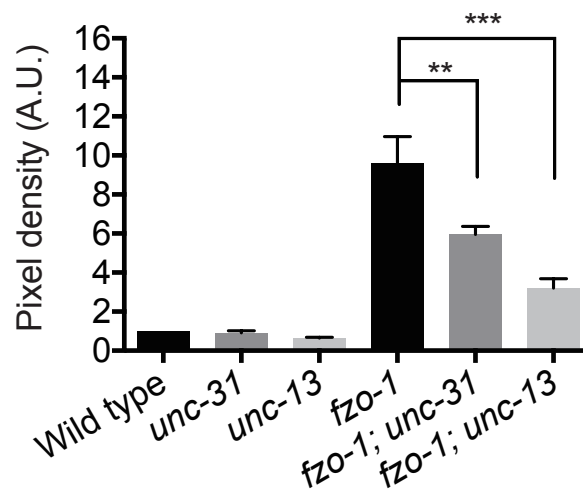
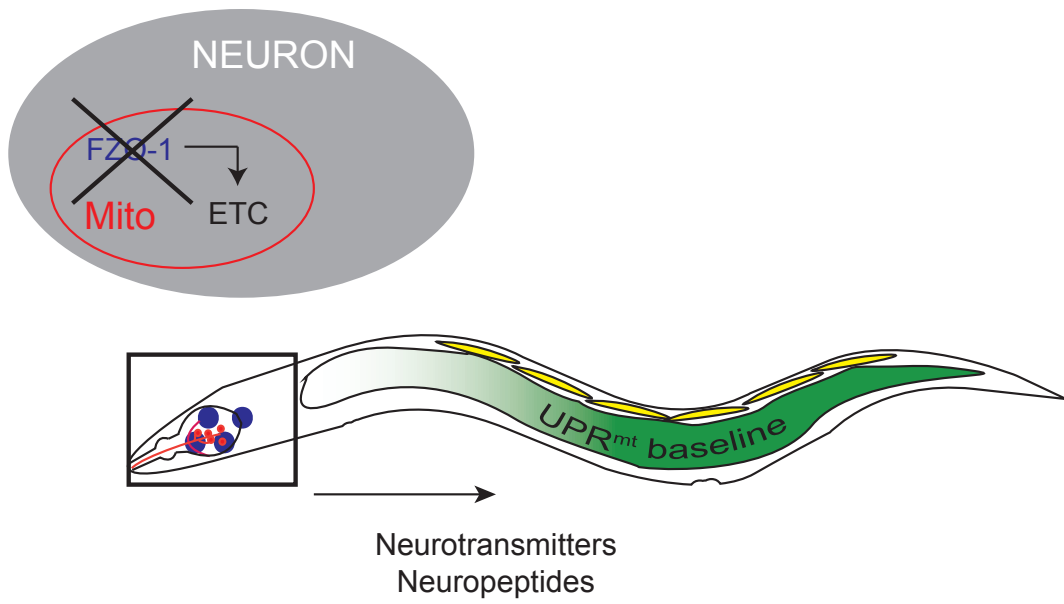


Figure 28. Model of systemic UPR^{mt} regulation by *fzo-1* in the neurons.







Chapter 6 REFERENCE



Balch, W.E., Morimoto, R.I., Dillin, A., and Kelly, J.W. (2008). Adapting proteostasis for disease intervention. *Science* 319, 916-919.

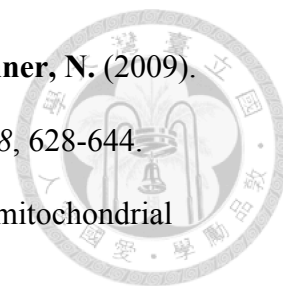
Benedetti, C., Haynes, C.M., Yang, Y., Harding, H.P., and Ron, D. (2006). Ubiquitin-like protein 5 positively regulates chaperone gene expression in the mitochondrial unfolded protein response. *Genetics* 174, 229-239.

Breckenridge, D.G., Kang, B.H., Kokel, D., Mitani, S., Staehelin, L.A., and Xue, D. (2008). *Caenorhabditis elegans* drp-1 and fis-2 regulate distinct cell-death execution pathways downstream of ced-3 and independent of ced-9. *Mol Cell* 31, 586-597.

Brenner, S. (1974). The genetics of *Caenorhabditis elegans*. *Genetics* 77, 71-94.

Burkewitz, K., Morantte, I., Weir, H.J., Yeo, R., Zhang, Y., Huynh, F.K., Ilkayeva, O.R., Hirschey, M.D., Grant, A.R., and Mair, W.B. (2015). Neuronal CRTC-1 governs systemic mitochondrial metabolism and lifespan via a catecholamine signal. *Cell* 160, 842-855.

Cartoni, R., Arnaud, E., Medard, J.J., Poirot, O., Courvoisier, D.S., Chrast, R., and Martinou, J.C. (2010). Expression of mitofusin 2(R94Q) in a transgenic mouse leads to Charcot-Marie-Tooth neuropathy type 2A. *Brain* 133, 1460-1469.



Chacinska, A., Koehler, C.M., Milenkovic, D., Lithgow, T., and Pfanner, N. (2009).

Importing mitochondrial proteins: machineries and mechanisms. *Cell* 138, 628-644.

Chan, D.C. (2012). Fusion and fission: interlinked processes critical for mitochondrial health. *Annu Rev Genet* 46, 265-287.

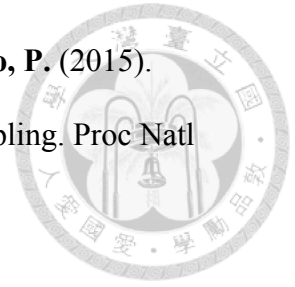
de Brito, O.M., and Scorrano, L. (2008). Mitofusin 2 tethers endoplasmic reticulum to mitochondria. *Nature* 456, 605-610.

Dillin, A., Hsu, A.L., Arantes-Oliveira, N., Lehrer-Graiwer, J., Hsin, H., Fraser, A.G., Kamath, R.S., Ahringer, J., and Kenyon, C. (2002). Rates of behavior and aging specified by mitochondrial function during development. *Science* 298, 2398-2401.

Durieux, J., Wolff, S., and Dillin, A. (2011). The cell-non-autonomous nature of electron transport chain-mediated longevity. *Cell* 144, 79-91.

Ehrenberg, B., Montana, V., Wei, M.D., Wuskell, J.P., and Loew, L.M. (1988). Membrane potential can be determined in individual cells from the nernstian distribution of cationic dyes. *Biophys J* 53, 785-794.

Ferri, K.F., and Kroemer, G. (2001). Organelle-specific initiation of cell death pathways. *Nat Cell Biol* 3, E255-263.



Filadi, R., Greotti, E., Turacchio, G., Luini, A., Pozzan, T., and Pizzo, P. (2015). Mitofusin 2 ablation increases endoplasmic reticulum-mitochondria coupling. *Proc Natl Acad Sci U S A* *112*, E2174-2181.

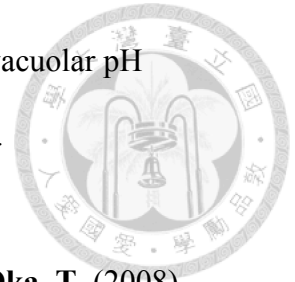
Haynes, C.M., Petrova, K., Benedetti, C., Yang, Y., and Ron, D. (2007). ClpP mediates activation of a mitochondrial unfolded protein response in *C. elegans*. *Dev Cell* *13*, 467-480.

Haynes, C.M., and Ron, D. (2010). The mitochondrial UPR - protecting organelle protein homeostasis. *J Cell Sci* *123*, 3849-3855.

Haynes, C.M., Yang, Y., Blais, S.P., Neubert, T.A., and Ron, D. (2010). The matrix peptide exporter HAF-1 signals a mitochondrial UPR by activating the transcription factor *ZC376.7* in *C. elegans*. *Mol Cell* *37*, 529-540.

Hill, K., Model, K., Ryan, M.T., Dietmeier, K., Martin, F., Wagner, R., and Pfanner, N. (1998). Tom40 forms the hydrophilic channel of the mitochondrial import pore for preproteins [see comment]. *Nature* *395*, 516-521.

Houtkooper, R.H., Mouchiroud, L., Ryu, D., Moullan, N., Katsyuba, E., Knott, G., Williams, R.W., and Auwerx, J. (2013). Mitonuclear protein imbalance as a conserved longevity mechanism. *Nature* *497*, 451-457.



Hughes, A.L., and Gottschling, D.E. (2012). An early age increase in vacuolar pH limits mitochondrial function and lifespan in yeast. *Nature* 492, 261-265.

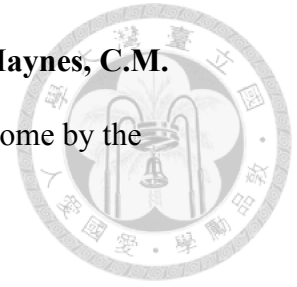
Ichishita, R., Tanaka, K., Sugiura, Y., Sayano, T., Mihara, K., and Oka, T. (2008). An RNAi screen for mitochondrial proteins required to maintain the morphology of the organelle in *Caenorhabditis elegans*. *J Biochem* 143, 449-454.

Jiang, H.C., Hsu, J.M., Yen, C.P., Chao, C.C., Chen, R.H., and Pan, C.L. (2015). Neural activity and CaMKII protect mitochondria from fragmentation in aging *Caenorhabditis elegans* neurons. *Proc Natl Acad Sci U S A* 112, 8768-8773.

Johnson, D., and Nehrke, K. (2010). Mitochondrial fragmentation leads to intracellular acidification in *Caenorhabditis elegans* and mammalian cells. *Mol Biol Cell* 21, 2191-2201.

Kamath, R.S., Martinez-Campos, M., Zipperlen, P., Fraser, A.G., and Ahringer, J. (2001). Effectiveness of specific RNA-mediated interference through ingested double-stranded RNA in *Caenorhabditis elegans*. *Genome Biol* 2, RESEARCH0002.

Lee, S.S., Lee, R.Y., Fraser, A.G., Kamath, R.S., Ahringer, J., and Ruvkun, G. (2003). A systematic RNAi screen identifies a critical role for mitochondria in *C. elegans* longevity. *Nat Genet* 33, 40-48.



Lin, Y.F., Schulz, A.M., Pellegrino, M.W., Lu, Y., Shaham, S., and Haynes, C.M. (2016). Maintenance and propagation of a deleterious mitochondrial genome by the mitochondrial unfolded protein response. *Nature* 533, 416-419.

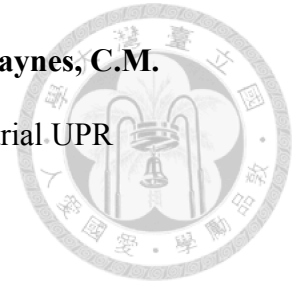
Madison, J.M., Nurrish, S., and Kaplan, J.M. (2005). UNC-13 interaction with syntaxin is required for synaptic transmission. *Curr Biol* 15, 2236-2242.

Mello, C.C., Kramer, J.M., Stinchcomb, D., and Ambros, V. (1991). Efficient gene transfer in *C.elegans*: extrachromosomal maintenance and integration of transforming sequences. *EMBO J* 10, 3959-3970.

Merkwirth, C., Jovaisaite, V., Durieux, J., Matilainen, O., Jordan, S.D., Quiros, P.M., Steffen, K.K., Williams, E.G., Mouchiroud, L., Tronnes, S.U., et al. (2016). Two Conserved Histone Demethylases Regulate Mitochondrial Stress-Induced Longevity. *Cell* 165, 1209-1223.

Munoz, J.P., Ivanova, S., Sanchez-Wandelmer, J., Martinez-Cristobal, P., Noguera, E., Sancho, A., Diaz-Ramos, A., Hernandez-Alvarez, M.I., Sebastian, D., Mauvezin, C., et al. (2013). Mfn2 modulates the UPR and mitochondrial function via repression of PERK. *EMBO J* 32, 2348-2361.

Nargund, A.M., Fiorese, C.J., Pellegrino, M.W., Deng, P., and Haynes, C.M. (2015). Mitochondrial and nuclear accumulation of the transcription factor ATFS-1 promotes OXPHOS recovery during the UPR(mt). *Mol Cell* 58, 123-133.



Nargund, A.M., Pellegrino, M.W., Fiorese, C.J., Baker, B.M., and Haynes, C.M. (2012). Mitochondrial import efficiency of ATFS-1 regulates mitochondrial UPR activation. *Science* 337, 587-590.

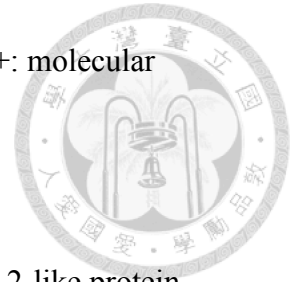
Nolden, M., Ehses, S., Koppen, M., Bernacchia, A., Rugarli, E.I., and Langer, T. (2005). The m-AAA protease defective in hereditary spastic paraplegia controls ribosome assembly in mitochondria. *Cell* 123, 277-289.

Pan, C.L., Peng, C.Y., Chen, C.H., and McIntire, S. (2011). Genetic analysis of age-dependent defects of the *Caenorhabditis elegans* touch receptor neurons. *Proc Natl Acad Sci U S A* 108, 9274-9279.

Pellegrino, M.W., Nargund, A.M., Kirienko, N.V., Gillis, R., Fiorese, C.J., and Haynes, C.M. (2014). Mitochondrial UPR-regulated innate immunity provides resistance to pathogen infection. *Nature* 516, 414-417.

Prahlad, V., Cornelius, T., and Morimoto, R.I. (2008). Regulation of the cellular heat shock response in *Caenorhabditis elegans* by thermosensory neurons. *Science* 320, 811-814.

Raj, A., van den Bogaard, P., Rifkin, S.A., van Oudenaarden, A., and Tyagi, S. (2008). Imaging individual mRNA molecules using multiple singly labeled probes. *Nat Methods* 5, 877-879.



Rizzuto, R., and Pozzan, T. (2006). Microdomains of intracellular Ca²⁺: molecular determinants and functional consequences. *Physiol Rev* 86, 369-408.

Rolland, S.G., Lu, Y., David, C.N., and Conradt, B. (2009). The BCL-2-like protein CED-9 of *C. elegans* promotes FZO-1/Mfn1,2- and EAT-3/Opa1-dependent mitochondrial fusion. *J Cell Biol* 186, 525-540.

Rossor, A.M., Polke, J.M., Houlden, H., and Reilly, M.M. (2013). Clinical implications of genetic advances in Charcot-Marie-Tooth disease. *Nat Rev Neurol* 9, 562-571.

Roux, A.E., Langhans, K., Huynh, W., and Kenyon, C. (2016). Reversible Age-Related Phenotypes Induced during Larval Quiescence in *C. elegans*. *Cell Metab* 23, 1113-1126.

Scheckhuber, C.Q., Erjavec, N., Tinazli, A., Hamann, A., Nystrom, T., and Osiewacz, H.D. (2007). Reducing mitochondrial fission results in increased life span and fitness of two fungal ageing models. *Nat Cell Biol* 9, 99-105.

Schieber, M., and Chandel, N.S. (2014). TOR signaling couples oxygen sensing to lifespan in *C. elegans*. *Cell Rep* 9, 9-15.

Schneeberger, M., Dietrich, M.O., Sebastian, D., Imbernon, M., Castano, C., Garcia, A., Esteban, Y., Gonzalez-Franquesa, A., Rodriguez, I.C., Bortolozzi, A., et



al. (2013). Mitofusin 2 in POMC neurons connects ER stress with leptin resistance and energy imbalance. *Cell* 155, 172-187.

Speese, S., Petrie, M., Schuske, K., Ailion, M., Ann, K., Iwasaki, K., Jorgensen, E.M., and Martin, T.F. (2007). UNC-31 (CAPS) is required for dense-core vesicle but not synaptic vesicle exocytosis in *Caenorhabditis elegans*. *J Neurosci* 27, 6150-6162.

Tank, E.M., Rodgers, K.E., and Kenyon, C. (2011). Spontaneous age-related neurite branching in *Caenorhabditis elegans*. *J Neurosci* 31, 9279-9288.

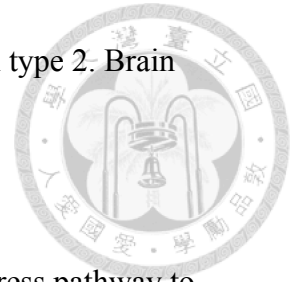
Tatum, M.C., Ooi, F.K., Chikka, M.R., Chauve, L., Martinez-Velazquez, L.A., Steinbusch, H.W., Morimoto, R.I., and Prahlad, V. (2015). Neuronal serotonin release triggers the heat shock response in *C. elegans* in the absence of temperature increase. *Curr Biol* 25, 163-174.

Taylor, R.C., and Dillin, A. (2013). XBP-1 is a cell-nonautonomous regulator of stress resistance and longevity. *Cell* 153, 1435-1447.

Toth, M.L., Melentijevic, I., Shah, L., Bhatia, A., Lu, K., Talwar, A., Naji, H., Ibanez-Ventoso, C., Ghose, P., Jevince, A., et al. (2012). Neurite sprouting and synapse deterioration in the aging *Caenorhabditis elegans* nervous system. *J Neurosci* 32, 8778-8790.

Verhoeven, K., Claeys, K.G., Zuchner, S., Schroder, J.M., Weis, J., Ceuterick, C., Jordanova, A., Nelis, E., De Vriendt, E., Van Hul, M., et al. (2006). MFN2 mutation

distribution and genotype/phenotype correlation in Charcot-Marie-Tooth type 2. *Brain* 129, 2093-2102.



Walter, P., and Ron, D. (2011). The unfolded protein response: from stress pathway to homeostatic regulation. *Science* 334, 1081-1086.

Yasuda, K., Ishii, T., Suda, H., Akatsuka, A., Hartman, P.S., Goto, S., Miyazawa, M., and Ishii, N. (2006). Age-related changes of mitochondrial structure and function in *Caenorhabditis elegans*. *Mech Ageing Dev* 127, 763-770.

Yoneda, T., Benedetti, C., Urano, F., Clark, S.G., Harding, H.P., and Ron, D. (2004). Compartment-specific perturbation of protein handling activates genes encoding mitochondrial chaperones. *J Cell Sci* 117, 4055-4066.

Young, L., Leonhard, K., Tatsuta, T., Trowsdale, J., and Langer, T. (2001). Role of the ABC transporter Mdl1 in peptide export from mitochondria. *Science* 291, 2135-2138.

Zuchner, S., Mersiyanova, I.V., Muglia, M., Bissar-Tadmouri, N., Rochelle, J., Dadali, E.L., Zappia, M., Nelis, E., Patitucci, A., Senderek, J., et al. (2004). Mutations in the mitochondrial GTPase mitofusin 2 cause Charcot-Marie-Tooth neuropathy type 2A. *Nat Genet* 36, 449-451.